ABSTRACT

Functional and cellular assessment of limited remyelination in the cuprizone model

Norah E. Hibbits, Doctor of Philosophy 2012

Thesis directed by: Dr. Regina Armstrong, Professor, Department of Anatomy, Physiology and Genetics

The promotion of remyelination after chronic or prolonged episodes of demyelination is an important therapeutic goal for demyelinating diseases. The leading cause of demyelination in humans is multiple sclerosis (MS). This thesis work focused on a mouse model of MS to examine cellular and molecular mechanisms that may cause limited remyelination after chronic demyelination. Cuprizone, a neurotoxicant, was used to induce experimental demyelination. This model mimics the effects of acute and chronic time courses of demyelinating disease progression. The cuprizone model facilitates identification and characterization of cellular mechanisms that may contribute to the limited remyelination observed during recovery from chronic demyelination. In this work, quantification of TUNEL staining indicated that apoptosis is ongoing during a recovery period following chronic demyelination. The observed ongoing apoptosis partially affects oligodendrocyte lineage cells, the myelinating cells of the central nervous system (CNS). This indicates that apoptosis may contribute to the

limited repair capacity following chronic demyelination. Further studies were performed to characterize the astroglial response as another potential contributor to recovery following acute and chronic demyelination paradigms. Histopathology, immunohistochemistry, as well as real-time quantitative (RT-Q) PCR was used to demonstrate progression of severe diffuse reactive astrogliosis without formation of a compact glial scar. Moreover, a constellation of astroglial-related genes was identified with the potential to influence the oligodendrocyte lineage (OL) cell response to demyelination. A functional non-invasive targeted behavioral assay was developed as means of assessing demyelination status in the mouse corpus callosum (CC) during cuprizone treatment. Both a sensorimotor running wheel task and a resident-intruder social interaction paradigm were shown to reliably phenotype small cohorts of mice according to demyelination status. The work presented has implications for the diagnosis of remyelination potential in demyelinated lesions as well as for the design and testing of novel therapeutics to promote functional remyelination.

FUNCTIONAL AND CELLULAR ASSESSMENT OF LIMITED REMYELINATION IN THE CUPRIZONE MODEL

by

Norah E. Hibbits

Dissertation submitted to the Faculty of the
Neuroscience Graduate Program
Uniformed Services University of the Health Sciences
in partial fulfillment of the requirements for the degree of
Doctor of Philosophy 2012

Table of Contents*

*Calibri (12) font is the default for this work
Times New Roman (12) indicates excerpts from (Hibbits et al., 2009)

List of Abbreviations

ANOVA – analysis of variance
av - arbor vitae
bp – base pair
C - complex
CC – corpus callosum
cDNA – complementary deoxyribonucleic acid
cg - cingulum
CNS – central nervous system
Col8a2 – collagen gene
CSPG – chondroitin sulfate glycoprotein
Cy3 - indocarbocyanine
cx – cerebellar cortex
dhc – dorsal hippocampal commissure
dUTP – deoxyuridine triphosphate
DAPI – 4', 6' diamidino-2 -phenylindole
ECM – extracellular matrix
Fgf2 – fibroblast growth factor 2
Fn1 – fibronectin gene
GFAP – glial fibrillary acidic protein
h - hilus
hPDGF – human platelet derived growth factor
IgG – immunoglobulin G
IgM – immunoglobulin M
LFB – Luxol Fast Blue
MAG- myelin associated glycoprotein
MBP – myelin basic protein
MOG – myelin oligodendrocyte glycoprotein
MOSS – motor skills sequence
mRNA – messenger ribonucleic acid
MS – multiple sclerosis
"n" – number (usually amount of animals in analysis)
Nes – nestin
NBT/BCIP - nitro-blue tetrazolium chloride/5-bromo-4-chloro-3'-indolyphosphate p-toluidine salt
OH - hydroxyl
OL – oligodendrocyte lineage
Olig2 – oligodendrocyte transcription factor 2
PDGFaR – platelet derived growth factor receptor alpha
PDGF-A – platelet derived growth factor A (ligand)
PLP – proteolipid protein
RNA – ribonucleic acid
RT-QPCR – quantitative real-time polymerase chain reaction
s.d. – standard deviation
s.e.m. – standard error of the mean
sl – stratum lacunosum of CA1
SVG – subgranular zone
SVZ – subventricular zone
T - training
TdT – terminal deoxynucleotidyl transferase
Tg - transgenic
Tnc – tenascin c
TUNEL – terminal deoxynucleotidyl transferase
USUHS – Uniformed Services University of the Health Sciences
um - micron
Vmax – maximum velocity
w/w – weight/weight
wt – wild-type
ΔΔCt – delta delta cycle threshold

List of Tables

List of Figures

Chapter I: Introduction

Statement of Problem

Demyelination, the loss of oligodendroglial cells ensheathing axons is a serious impairment that leads to reduced conduction for neuronal signaling. Ultimately, lost neuronal signaling conduction results in impairments of motor and/or cognitive function. There are many causes of demyelination in the central nervous system (CNS), including injury, toxins, neurodegeneration and disease. The most prevalent cause of demyelination is multiple sclerosis (MS). MS affects nearly two million people worldwide (Milo and Kahana, 2009). MS usually presents early in life and is the leading cause of neurologic disability among young adults (Milo and Kahana, 2009). The most common form of MS has a relapsing-remitting pattern of symptoms. This means that in early stages of the MS disease course there is spontaneous repair, which occurs via remyelination. Remyelination is growth of myelinating oligodendrocytes to ensheath axons denuded during demyelination. This observed spontaneous repair, termed remission, often produces restored function in the patient. However, as the disease progresses, demyelinating events become more prolonged and chronically occurring. The amount of spontaneous remyelination and repair subsequently diminishes. Current therapies for MS treat symptoms as they arise and also help delay the onset of relapses (Payne et al., 2011). However, few therapies focus on promoting repair in the later stages of the disease course. Research to promote remyelination after chronic and prolonged episodes of demyelination, therefore, is an essential therapeutic goal for MS and other demyelinating disorders.

Specific Aims

In this work a rodent model of demyelination was used to address the problem of promoting remyelination after chronic or prolonged episodes of demyelination. Within this work there are three specific aims. In the first specific aim the particular cellular aspect studied is apoptosis. Apoptosis, or programmed cell death is a ubiquitous cellular mechanism that directly regulates cell survival. OL cells might undergo apoptosis in the context of either chronic demyelination, or recovery from chronic demyelination. Thus, apoptosis could be a contributor to limited repair after chronic demyelination. The first specific aim of this work is therefore to determine the *in vivo* contribution of apoptosis on limited repair after chronic demyelination.

The second specific aim of this work moves from the cellular and molecular level of study up to the neural circuit and systems level of study. At this level of study, the interplay between cell types is important. The astrocytic network, composed of astrocytes, a particular type of glia cell, can be considered a neuronal system. Similarly, oligodendrocytes, the myelinating glia cells of the CNS, might be considered a separate neuronal system. Since no one neuronal system is entirely independent, it is important to recognize the influences each neuronal system has on other neuronal systems. In this work, interest centers on oligodendrocytes and their capacity for remyelination. The link between the astroglial neuronal system and the oligodendroglial system is not well established. The second aim of this work is consequently to characterize the astroglial response in acute and chronic corpus callosum demyelination relative to the oligodendroglial lineage. That is, the second aim of this work intends to describe the dynamics

of the astroglial response as a corollary to the changes in the OL response during demyelination.

The third specific aim of this work moves from the neuronal circuits and systems level of study up to the cognitive and behavioral level of study. At this level of study, the organism as a whole is examined. In this work, the question raised pertains to limited remyelination after chronic or prolonged episodes of demyelination. With examination of the entire organism, this translates to functional behavioral correlates of demyelination status. Thus, the third specific aim in this work is to develop and test a targeted non-invasive assay for mouse demyelination that can be used in longitudinal studies to assess repair. Rodents, specifically mice, are the most commonly used model organism for research on demyelination. An established non-invasive behavioral assay would allow assessment of demyelination status without sacrificing the mouse. Additionally, such an assay should be targeted to detect demyelination in a specific lesion area. In this manner the assay would correspond well with deficits specifically associated with demyelination. That is, systemic effects from the method used to induce demyelination should not affect the outcome of assay. Such a targeted non-invasive assay could be used to assess functional recovery over time. Moreover, therapeutics designed to promote the enhancement of limited remyelination after chronic or prolonged demyelination could be tested using such a targeted non-invasive assay for mouse demyelination.

Literature Review

Terminology

MS is the leading cause of neurologic disability among young adults (Milo and Kahana, 2009). The hallmark symptom of MS is focal demyelination. Symptoms arise based not only on the degree of demyelination during MS progression, but also based on the location of the lesion. Demyelination can occur throughout the CNS, but large white matter tracts with large numbers of mature oligodendrocytes are often affected. In fact, the corpus callosum (CC) represents the largest white matter tract in the brain. Nearly 90 percent of patients with MS exhibit lesions in the CC area (Gean-Marton et al., 1991). Some common symptoms of MS include tingling, numbness, loss of balance and blurred or double vision.

The cause of MS symptoms is attributed to impaired neuronal conduction. Impaired neuronal conduction is a direct result of demyelination. Myelin not only insulates neuronal axons, but also facilitates efficient electrical signaling along axons. That is, without sufficient myelin, there is reduced axonal conduction, reducing reaction time within the CNS. Continued impairment in neuronal conduction leaves axons vulnerable to atrophy due to lack of trophic support. Axonal atrophy corresponds with more severe neurological deficits and also with increased difficulty for repair and functional recovery (Lassmann, 2011).

In addition to focal demyelination, MS is associated with inflammation at the lesion area (Nakahara et al., 2010). There is a debate as to whether inflammation is the primary cause of demyelination in MS or whether demyelination is the primary event in the pathogenesis of MS (Nakahara et al., 2010). In either case, demyelination and inflammation are intricately linked during the course of MS. Research into the destructive effects of demyelinating insults as well

as a possible link to subsequent inflammatory responses is useful for determining the mechanisms underlying MS.

While the initiating cause of MS is unknown, the disease progresses due to demyelination. A simplistic definition of demyelination is the loss of myelin sheaths surrounding axons. To better understand this definition myelin must first be described. Myelin is the fatty substance that covers neuronal axons. Myelin sheaths in the CNS are generated from the outgrowth of processes from a specific type of glia cell. These glia cells are called oligodendrocytes. One oligodendrocyte cell has the ability to myelinate several different neuronal axons through the outgrowth of many processes. The major purpose of myelin sheaths is to facilitate neurotransmission along axons. Without myelin the speed of neurotransmission would be significantly slower (Hartline and Colman, 2007). Indeed, when there is demyelination, axonal conduction slows. This leads to a variety of neurologic impairments including motor and/or cognitive disturbances.

As mentioned, oligodendrocytes are a specific type of glia cell within the CNS. Glia is a Latin word that literally means “glue”. The term glia arose to describe the support cells in the CNS. Indeed, glia cells do serve a supportive function. They fill the space around neurons, which are the electrically active cells in the CNS responsible for signal transduction. Though glia cells usually do not act to propagate neurotransmission, glia cells do serve many important functions in the CNS.

Many functions of glia cells are served by a specialized cell type. For instance, microglia are the smallest glia of the cells. They are specifically suited to serve the function of cleaning up

cellular debris within the CNS. Furthermore, they act as the phagocytic cells of the brain. In healthy tissue, microglia are dispersed throughout the CNS. Upon injury, microglia cells become activated with morphological and phenotypical changes. Other types of glia cells important in this work include astrocytes and oligodendrocytes.

Astrocytes are the most abundant glia cell type in the brain. They serve a variety of functions. Astrocytes are especially important in maintaining homeostasis within the CNS, particularly in the context of health and disease (Albrecht et al., 2003; Williams et al., 2007; Sofroniew and Vinters, 2010). Morphologically, astrocytes are the largest glia cells. Generally astrocytes are star-shaped and become hypertrophic in response to injury within the CNS.

Oligodendrocytes, as mentioned briefly, are a specialized type of glia cell that form the myelin sheaths in the brain. Myelin is an outgrowth of processes from mature fully differentiated oligodendrocyte cells. The loss of these mature oligodendroglial cells results in demyelination, the loss of myelin sheaths. Remyelination on the other hand, is the maturation of oligodendrocyte lineage cells into myelinating sheaths surrounding axons. A secondary role of the myelin sheath is to protect axons from damage. Remyelination can enhance restoration of function and also act as a method of neuroprotection for axons in the brain.

While it is mature, fully differentiated oligodendrocytes that form the myelin sheaths within the CNS, oligodendrocyte progenitors are also particularly important for myelination. Oligodendrocyte progenitors are the precursors to mature oligodendrocytes. They arise from a multi-potent neural stem cell population (Gallo and Armstrong, 2008; Miron et al., 2011). Multi-potent progenitors are found to some degree dispersed throughout the CNS. However, the

majority of these progenitor cells are localized to specific neurogenic regions, such as the subventricular zone (SVZ) (Gallo and Armstrong, 2008). The progression to fully mature myelinating oligodendrocyte cells can be characterized based on various morphological and phenotypical changes. For instance, multi-potent progenitor cells have a round appearance with few processes. Such multi-potent progenitor cells express nestin, which is an intermediate filament protein. In contrast, oligodendrocyte progenitor cells tend to have bipolar processes and express among other factors, platelet derived growth factor receptor alpha (PDGFaR) (Miron et al., 2011). OL cell progression continues then from oligodendrocyte progenitors to pre and immature oligodendrocyte lineage cells expressing O4 and GalC (Miron et al., 2011). Once mature, oligodendrocytes have several myelinating processes and express many different myelin-related proteins such as myelin basic protein (MBP), myelin-associated glycoprotein (MAG) and myelin oligodendrocyte glycoprotein (MOG) (Miron et al., 2011). Throughout progression from immature to mature oligodendrocytes Olig2 can detected, making it a good marker for all stages of the oligodendrocyte cell lineage (Vana et al., 2007; Miron et al., 2011).

Importance of CC demyelination

The CC is the largest white matter tract in the brain and is the target of many animal models of demyelination and remyelination via injection of toxins or antibodies or by ingestion of cuprizone (Gensert and Goldman, 1997; Matsushima and Morell, 2001; Armstrong et al., 2002; Decker et al., 2002). In addition to being a target for animal studies of demyelination, the CC is implicated in human demyelinating diseases. The CC is important for transfer and integration of information between the two hemispheres of the brain. Humans with agenesis of

the CC have normal intelligence, but present with subtle cognitive deficits, especially in language ability (Paul et al., 2007). Similar deficits are also observed in patients that have undergone callosotomy (Devinsky and Laff, 2003). Such language deficits are associated with problems in social interaction and are symptoms of the autism spectrum disorders (Paul et al., 2007).

In addition to language deficits, CC structural abnormalities have shown a correlation with impairments in motor tasks involving bimanual finger coordination. These motor impairments are observed in patients with agenesis of the CC, in patients that have undergone callosotomy, in children in whom the CC is not fully myelinated, and also in MS patients (Kennerley et al., 2002; Bonzano et al., 2008; Muetzel et al., 2008).

In addition to being the largest white matter tract in the brain and exhibiting functional biological deficits when impaired in humans, the CC is also a beneficial model for demyelination studies due to its location. The CC is located adjacent to the subventricular zone, a potential source for neural stem cells (Gallo and Armstrong, 2008). This makes the CC ideally located to monitor neuroregenerative responses for repair of demyelination.

MS disease progression

Research to promote remyelination after chronic or prolonged episodes of demyelination is a promising field. Remission in the context of MS shows that spontaneous remyelination and functional recovery can occur, at least in the early stages of demyelination. Functional remyelination is less extensive in chronic MS, but still occurs (Prineas, Connell, 1979). In fact, some subsets of patients with chronic MS exhibit almost complete remyelination within

previously demyelinated white matter (Patrikos, 2006). While this shows that remyelination is possible in the context of chronic disease, remyelination tends to fail as the disease progresses in the majority of MS cases (Patrikos, 2006, Patani et al, 2007). Furthermore, this suggests that the micro-environment within chronic MS limits remyelination (Gallo and Armstrong, 2008). Moreover, OL cells likely retain the ability to remyelinate denuded axons even in the context of chronic demyelination (Patani et al, 2007).

The potential for remyelination is partially influenced by the temporal dynamics involved in the disease course of MS. Although a relapsing-remitting disease course is the most common form of MS, it can also present as a primary progressive disease with continual worsening of symptoms and no distinct remission period (Antel et al., 2012). Indeed, 50-60 percent of relapsing-remitting MS cases progress from relapsing-remitting to secondary progressive MS (Antel et al, 2012). Although lesion status in MS is not a direct indicator of disability, continuous demyelination over time could contribute to a greater lesion load. A greater lesion load means a higher potential for axonal damage or loss, markers that do correlate more closely with disability (Schirmer et al., 2011). Furthermore, an effective means to prevent disability attributed to axonal damage or loss is to promote neuroprotection through mechanisms like remyelination (Karussis et al., 2006; Stangel, 2008).

Differences in disease course and symptom severity are likely due to variable lesion location, lesion number, and lesion volume as well as the extent of demyelination. Comparisons of remyelination between early and late disease courses show that remyelination is more

frequent in early stages of MS (Perier and Gregoire, 1965; Prineas and Connell, 1979; Prineas et al., 1993; Hanafy and Sloane, 2011).

Types of MS lesions

The potential for remyelination within MS lesions might partially depend on lesion status. Though all MS lesions possess several hallmark characteristics, such as primary demyelination with partial axonal preservation (Lassmann, 2011), MS lesions are not uniform. Indeed, descriptions of lesion activity in MS show that there can be six different types of lesions, characterized by the location and presence or absence of inflammation and demyelination (van der Valk and De Groot, 2000). The six types of lesions are labeled as 1) inflammatory (solid) and demyelinating, 2) inflammatory (solid) and not demyelinating, 3) inflammatory rim (hypocellular center) and demyelinating, 4) inflammatory rim (hypocellular center), not demyelinating, 5) no inflammation and demyelinating, 6) no inflammation and not demyelinating (van der Valk and De Groot, 2000). This classification scheme accurately describes all possible lesion types observed in MS, though some categories, namely category 5, do not seem likely (van der Valk and De Groot, 2000). The distinction between inflammation within the solid area of the lesion versus the rim of the lesion is an attempt to reconcile previous descriptions of MS lesions, which also characterize lesion activity, but rely on time-course suggestive terminology. In these previous MS lesion descriptions, it was noted that early demyelinating lesions display inflammation through the lesion core, thus termed inflammation (solid). In contrast, later stage lesions, termed chronic active, show myelin loss at the center of

the lesion, indicating the hypocellular description, along with inflammation surrounding the lesion area, indicating the inflammatory rim designation (van der Valk and De Groot, 2000).

The classification of MS lesions into one of the six categories described serves a descriptive purpose and does not indicate a time frame for lesion development through the disease course (van der Valk and De Groot, 2000). Thus, previous descriptions of MS lesions with time-course suggestive classifications do not correspond directly with the six lesion categories. However, comparison of the classification systems reveals that active lesions, exhibit both inflammation and demyelination. Alternately, chronic active lesions show inflammation without signs of ongoing demyelination. Furthermore, chronic inactive lesions do not exhibit signs of inflammation and may or may not exhibit ongoing demyelination. Additionally, there could be another preactive lesion stage that does not have signs of either inflammation or demyelination, but might be distinguished by other early events in MS pathology.

Heterogeneity within MS lesions

In addition to the temporal progression of MS lesions, suggested by the classification schemes described, the immunopathological profile of MS lesions can vary even within a defined subset of lesion activity (Lucchinetti 2000). Indeed, active demyelinating MS lesions have been characterized as falling into one of four patterns with different immunopathological profiles (Lucchinetti 2000). Lesions designated Type I and II MS lesions suggest T-cell mediated demyelination and the possible implication of inflammation in addition to demyelination (Lucchinetti et al., 2000). Lesions designated Type III and IV on the other hand, seem to suggest oligodendrocyte dysfunction possibly without primary inflammation (Lucchinetti et al., 2000).

Cellular determinants of remyelination capacity

Many different cellular factors contribute to the capacity for remyelination, but the OL response ultimately determines whether remyelination will occur. The response of OL progenitors is particularly important. OL progenitors are multipotent cells that eventually give rise to mature oligodendrocytes capable of myelination (Zhao et al., 2005; Gallo and Armstrong, 2008). While the majority of OL progenitors either differentiate or die off during development (Nguyen et al, 2006), a there is a population of OL progenitors that persists in the adult CNS. This cell population compromises from 5 to 8 percent of all cells in the adult brain (Levine et al, 2001). Without a robust OL progenitor response to demyelination, remyelination is unlikely as mature oligodendrocytes do not divide or contribute to remyelination (Keirstead, 1997, Redwine and Armstrong 1998, Di Bello et al, 1999).

There are four cellular properties that determine OL progenitor remyelination potential, i) proliferation, ii) migration, iii) differentiation and iv) survival. Proliferation is the capacity for early stage OL cells to divide and amplify. Early stage OL progenitor cells are found throughout the adult CNS, particularly in the SVZ, a neurogenic region of the brain, which can become activated after demyelinating insults (Gallo and Armstrong, 2008; Heneka et al., 2010). That is to say that demyelination can cause the neural progenitor pool to be expanded, including OL cells found in the SVZ. Furthermore, evidence suggests that OL progenitor cells and premyelinating oligodendrocytes can persist in MS lesions yet fail to efficiently remyelinate denuded axons (Wolswijk, 2000; Maeda et al., 2001; Wolswijk, 2002). Depletion of the oligodendrocyte progenitor pool and premyelinating oligodendrocyte populations as a

consequence of prolonged disease duration may limit the capacity for remyelination in chronic lesions (Wolswijk, 2000; Reynolds et al., 2001; Wolswijk, 2002; Mason et al., 2004). Migration is the ability for OL progenitor cells to move through the brain, particularly their ability to infiltrate lesion areas caused by demyelination. Even if OL progenitor cells exist in the brain and have the capacity for functional repair, they will not effectively remyelinate a lesion area if they cannot migrate to that lesion.

Differentiation is the transformation of OL progenitor cells into fully myelinating CNS cells that promote axonal conduction. To achieve successful remyelination OL cells must be able to grow into functional myelinating sheaths (Williams et al., 2007). Survival is an important factor at all OL stages. Without thriving OL cells, the chances for remyelination are diminished (Williams et al, 2007). Successful remyelination involves coordination of all four cellular properties mentioned. Conversely, limited remyelination might result from aberrations in one or more these cellular properties (Millet et al., 2009; Kotter et al., 2011; Moore et al., 2011).

Apoptosis in MS lesions

Apoptosis is a cellular mechanism capable of influencing OL capacity for remyelination as a direct means of regulating OL survival. In MS lesions, apoptosis is apparent (Dowling et al. 1997, Barnett and Prineas 2004). However, the majority of apoptosis occurring in MS lesions targets infiltrating inflammatory cells (Dowling et al, 1997). Still, some 14-40 percent of cells dying in MS lesions, either through necrosis or apoptosis have been identified as OL cells (Dowling et al, 1997). This indicates that OL cell death is an important component contributing to MS lesions. Indeed, apoptosis of mature OL cells has been observed as a characteristic of early and active

MS cases, suggesting that mature OL apoptosis is an early stage mediator of myelin loss in MS (Barnett and Prineas 2004).

The percent of dying OL cells observed in MS lesions might have such a broad range due to the heterogeneity of lesions (Lucchinetti et al., 1999, 2000; Lucchinetti and Bruck, 2004). Furthermore, apoptosis is a complex cellular process involving the interplay of many different signals and death receptors that initiate the process of apoptosis are observed in MS lesions (Cannella et al, 2007). This indicates that though apoptosis of OL cells in chronic MS lesions is not robust (Canella et al, 2007, Dowling et al, 1997), the machinery of apoptosis is present and might be activated a low levels. Moreover, the temporal characteristics of apoptosis are not well-defined (Muliyil et al., 2011). Thus, activation of death receptors on OL cells at early disease stages could produce apoptosis much later in disease progression.

Interestingly, OL apoptosis was observed only in one type of lesion designated Type III lesions (Luchinetti 2000). Four different types of MS lesions have been described based on differences in demyelination patterns and immunopathological profiles (Lucchinetti et al., 2000). Furthermore, a recent report (Breij et al., 2008) suggests that the heterogeneity in immunopathogical profiles described in early active MS lesions (Lucchinetti 2000) is only characteristic of very early disease states. Taken together, these results indicate that OL apoptosis might be a characteristic marker for early stage MS.

Manipulation of cellular factors to promote remyelination potential

Apoptosis, as a direct regulator of OL survival represents one avenue for manipulation of the OL progenitor response in the context of remyelination. The role of apoptosis on limited

remyelination after chronic demyelination is examined in this work. Other regulators of the cellular properties governing the OL response to demyelination examined in this work are not as direct. Both intrinsic temporal mechanisms, such as OL age and development, as well as extrinsic regulatory mechanisms, such as neuronal signaling, secretion of cytokines, growth and transcription factors have the potential to modulate the OL response in the context of demyelination (Millet et al 2009, Gallo and Armstrong 2008).

Specific manipulation of astrocytes to influence the degree of astroglial activity or other cellular mechanisms like apoptosis could be a therapeutic avenue for MS research. Identifying cellular targets for manipulation is the first step in designing such therapeutics and is the goal of both the first and second specific aims within this work. Though the ultimate goal is to design therapeutics for humans, controlled experiments are difficult in humans due to limited tissue samples and lack of control for confounding factors. Therefore it is useful to employ animal models to tease apart the mechanisms controlling limited remyelination after chronic or prolonged demyelination.

Astrogliosis as a potential contributor to remyelination potential

Astroglial activation, commonly referred to as astrogliosis, is a major contributor to the generation of extrinsic regulatory mechanisms for the OL response to demyelination. Astroglial activation can stimulate the production of various growth factors, cytokines and chemokines (Gallo and Armstrong, 2008). Such secreted factors can be either beneficial or detrimental to the OL capacity for remyelination in MS (Williams et al., 2007; Fitch and Silver, 2008; Gallo and Armstrong, 2008; Sofroniew, 2009; Hamby and Sofroniew, 2011). Indeed, astrogliosis has long

been recognized as a characteristic of MS lesions (Lucchinetti et al., 2012). Only recently has the effect of astroglial activation been brought into question with regards to the context of remyelination (Williams et al., 2007). Though activated astrocytes express several factors with the potential to influence OL cells, the expression pattern of such factors could vary widely based on the extent of astroglial activation within the continuum of astroglial activation (Sofroniew and Vinters 2010).

Characterizing the extent of astrogliosis during demyelination will therefore be helpful in determining the role that astrocytes play in influencing the OL response to demyelination. However, because the continuum of astroglial activation is defined as gradual changes in astrocyte morphology and phenotype expression, the boundaries for classifying the degree of astroglial activation are not clear-cut. Still, attempts are being been made to standardize the classification of the degree of astroglial activation (Sofroniew and Vinters 2010). Within the proposed classification scheme for astroglial activation, there are four general categories. The first category defines astrocytes within healthy CNS tissue. In this category, some, but not all astrocytes express glial fibrillary acidic protein (GFAP), an intermediate filament protein characteristic of astrocytic cells. Also in this first category of astrogliosis in healthy CNS tissue, astrocytes remain in well-defined non-lapping domains and there either no or very little proliferation of astrocytes (Sofroniew and Vinters, 2010). The second category is mild to moderate astrogliosis in which most astrocytes express GFAP, individual astrocytic domains are preserved and there is still no or little proliferation (Sofroniew and Vinters, 2010). The third category is severe diffuse reactive astrogliosis in which most astrocytes express GFAP. There begins to be an over-lap of individual astrocytic domains and proliferation of astrocytes is

apparent (Sofroniew and Vinters, 2010). The fourth and most extreme category is severe astrogliosis with compact glial scar formation. This category has all the characteristics of severe diffuse astrogliosis plus there is deposition of a dense collagen extracellular matrix (ECM) along the border of areas of tissue damage, possibly serving the function to wall off the injured tissue from inflammatory non-CNS cells that invade after injury (Sofroniew and Vinters 2010). In this work, the stage of astrogliosis following demyelination was characterized according to the described classification scheme (Sofroniew and Vinters, 2010).

Animal models of demyelination

There are many animal models that induce demyelination (van der Goes and Dijkstra, 2001) and mice are the prototypical organism used for such research. Animal models are useful tools for studying the mechanisms of demyelination since there is a limited availability of human tissue for analysis. Additionally, animal studies offer greater control over confounding factors compared to human tissue samples. Mice are the prototypical animals used for studies of demyelination as they are readily available from commercial sources, have an immunological profile similar to humans and have been characterized using genetic manipulations.

There are three main groups of demyelination models in mice. These include autoimmune induced models of demyelination, viral induced models of demyelination and toxin induced models of demyelination (Denic et al., 2011). While each of these demyelinating models is important for uncovering the mechanisms of MS, it is important to note the limitations of these models. That is, no one demyelinating model is a perfect example of MS pathogenesis. Therefore it is important to define the aims of the study prior to choosing a demyelination

model. For studies of demyelination without a primary immune response, the cuprizone model is a good model (Kipp et al., 2009; Kotter et al., 2011).

The cuprizone model of demyelination

Cuprizone is neurotoxicant and copper chelator that when ingested specifically and reproducibly produces demyelination in the corpus callosum (CC) of male C57bl/6 mice (Mason et al., 2001; Matsushima and Morell, 2001; Armstrong et al., 2002; Armstrong et al., 2006). Moreover, cuprizone can be used to assess demyelination through different time-courses. Spontaneous remyelination is observed when mice are returned to normal chow for a designated recovery period. This feature of cuprizone ingestion has been used to answer different questions regarding demyelination and remyelination dynamics.

In general, cuprizone ingestion causes decreased axonal conduction by 2 weeks (Crawford et al., 2009) and maximal OL cell loss by 4 weeks of feeding at 0.2% (Matsushima and Morell, 2001). By 6 weeks of cuprizone ingestion, there is substantial myelin loss in the CC. When mice are allowed to return to normal chow for a recovery period after cuprizone ingestion, increases in OL proliferation occur quickly with recovery on normal chow there is significant remyelination (Matsushima and Morell, 2001). Alternatively, when mice are fed cuprizone for a chronic 12 week period, there is substantial myelin loss in the CC. However, returning those mice to normal chow for a 6 week recovery period results in remyelination that is limited compared to the acute recovery time-course (Armstrong et al., 2006; Hibbits et al., 2009). After cuprizone induced chronic demyelination, it has been shown that axons remain viable and can be remyelinated by transplanted OL progenitor cells (Mason et al., 2004).

Relative abundance of different cell type in the CC

As mentioned, the CC is an important area for studies of demyelination. Targeting of the CC with demyelinating models like cuprizone can help uncover mechanisms underlying MS and other demyelinating diseases. However, it is important to note that OL cells are not the only cell type found within the CC. Mature oligodendrocytes compromise more than half the cells found within the healthy mouse CC (Mason et al., 2000). A much smaller number of OL progenitor cells, compromising around 5 percent of the cell population of the healthy mouse CC, is also observable (Mason et al., 2000; Armstrong et al., 2006). Other cell types found in the healthy mouse CC include astrocytes, accounting for approximately 20 percent of the cell density as well as microglia, making up around 2 percent of the cell density in the healthy mouse CC (Mason et al., 2000; Steelman et al., 2012).

Upon cuprizone intoxication, the cellular density of the CC increases in mice (Hiremath et al., 1998). In fact, by 6 weeks of acute cuprizone demyelination, the number of cells in the CC nearly doubles (Hiremath et al., 1998). This increase in the number of cells in the mouse CC occurs despite a decrease in the number of mature, fully myelinating oligodendrocyte cells (Hiremath et al., 1998; Mason et al., 2000; Armstrong et al., 2006). The number of OL progenitor cells on the other hand, increases nearly 30 fold upon acute cuprizone ingestion (Mason et al., 2000; Armstrong et al., 2006). The density of microglia cells and to a lesser degree astrocytes also increase in response to cuprizone demyelination (Mason et al., 2004; Steelman et al., 2011). The cellular density of the CC has not been as well characterized upon chronic cuprizone ingestion. However, there is no continuation of increasing cell densities with

continued cuprizone ingestion. Rather, the cellular response seems to peak or plateau around 6 weeks of cuprizone ingestion (Mason et al., 2004; Xie et al., 2010).

Necessity for functional CC assays in rodents

A limitation of the CC as a model of demyelination is the lack of accepted functional measures to non-invasively monitor the effect of demyelination, especially for longitudinal studies. A behavioral assessment that correlates with demyelination in the mouse CC would provide insights into the role of the CC in rodents. Moreover, a behavioral assessment of CC function would facilitate non-invasive evaluation of CC demyelination for longitudinal studies throughout demyelination and remyelination. Importantly, a behavioral assay correlating with CC pathology is necessary to quantify deficits during acute demyelination and to subsequently test strategies to promote remyelination. This work used cuprizone administration to test two behavioral measures targeted for likely involvement of the CC, a bilateral sensorimotor running wheel task and a resident-intruder social interaction task.

Introduction overview

In the following pages cellular to systems to behavioral analyses will be used to examine potential mechanisms to enhance limited repair after chronic or prolonged demyelination. Apoptosis will be shown to be a contributor *in vivo* to the limited repair response after chronic demyelination. Astrogliosis will be characterized as occurring to the extent of severe diffuse reactive astrogliosis without compact glia scar formation. Finally, a functional, targeted and non-invasive behavioral assay will be described to detect demyelination status in mice.

Chapter II: Overview of experimental research methods

The methods that follow are a summary of similar methods used in all three specific aims addressed of this work. Detailed methods pertaining to each aim will follow in the results chapter for each specific aim.

Cuprizone experimental demyelination

Unlike other models of demyelination, cuprizone ingestion yields highly reproducible patterns of demyelination specifically in the mouse CC (Matsushima and Morell, 2001; Armstrong et al., 2002). This pattern of demyelination can be summarized as that acute cuprizone administration, for a relatively short, 6 week time-period is subsequently followed by spontaneous remyelination during a recovery time-period on normal chow. In contrast, remyelination becomes limited after the same recovery time-period following chronic cuprizone administration, for a longer 12 week time-period (Mason et al., 2001; Mason et al., 2004; Armstrong et al., 2006).

All the specific aims in this work utilize cuprizone ingestion to induce demyelination. The time-courses of cuprizone ingestion examined varied slightly between specific aims. For all three specific aims, 8 week old male mice were started on 0.2% (w/w) cuprizone diet (finely powdered oxalic bis (cyclohexylidenehydrazide); Sigma-Aldrich, Milwaukee, WI) mixed into milled chow (Harland Teklad, Certified LM-485 code 7012CM). Access to food was available *ad libitum*. Control mice were treated identically as mice receiving cuprizone, but were fed normal chow without cuprizone.

Tissue preparation

In all three specific aims, a subset, if not all experimental mice were intracardially perfused with 4% paraformaldehyde (Sigma, St. Louis, MO). Brains were then dissected prior to post-fixation in 4% paraformaldehyde at 4^{o}C overnight (Redwine and Armstrong, 1998). Tissue from the brains was then cryoprotected in 30% sucrose (Sigma, St. Louis, MO) at 4^{o}C overnight, embedded in Tissue Tek OCT (Sakura, Torrance, CA) and stored at –80^{o}C. For analysis with *in situ* hybridization, histopathology or immunohistochemistry coronal brain sections were cut at 15 μm on a cryostat and mounted onto Superfrost Plus slides (Fisher, Pittsburgh, PA).

Immunohistochemistry for myelin status

MOG is a late marker of fully mature oligodendrocytes (Coffey and McDermott, 1997). Its expression corresponds with both Luxol Fast Blue (LFB) and electron microscopic quantification of myelination better than the expression of either proteolipid protein (PLP) or MBP (Lindner et al., 2008). Both PLP and MBP are markers of mature oligodendrocytes, but are observed temporally earlier than MOG expression. LFB staining is a histological stain that stains myelin a blue color and is easily observable with light microscopy. LFB staining as well as detection of PLP, MBP and MOG have all been proposed as measures of myelination status during cuprizone ingestion (Lindner et al., 2008). Yet, the most reliable measure of myelination status in response to demyelinating insults remains electron microscopy (Lindner et al., 2008). Because MOG immunostaining in our lab corresponds well with previous LFB analyses, as well as electron microscopy analyses, MOG can be used as an indicator of myelination status during cuprizone ingestion (Armstrong et al., 2006; Hibbits et al., 2009; Xie et al., 2010)..

In all three specific aims, MOG was detected with the monoclonal antibody 8-18C5 (Dr Minettia Gardinier, University of Iowa, Iowa City, IA) followed by incubation with donkey anti-mouse IgG $F(ab)_2$ conjugated with Cy3 (Jackson Immunoresearch, West Grove, PA) (Armstrong et al., 2006). CC myelination status was estimated based on the area of MOG immunostaining quantified in coronal sections (Armstrong, 2006).

Imaging and quantification

Panel images presented were acquired with Spot2 software from a digital camera combined with an IX-70 inverted microscope (Olympus, Melville, NY). The panels were created using Adobe Photoshop (Mountain View, CA). For quantitative CC analyses the white matter of the body of the corpus callosum area between the midline and extending to below the apex of the cingulum on each side was used. Quantification of myelination of this corpus callosal area was then estimated from MOG immunofluorescence, which was detected with a narrow band pass filter for Cy3 (Chroma Technologies, Brattleboro, VT). To normalize pixel intensity values between sections, the Metamorph software package (Molecular Devices Corp., Downingtown, PA), was used. With this software, thresholding was performed to exclude values below the level of MOG immunoreactivity in the dorsal fornix, which is found just inferior to the CC and is not demyelinated by cuprizone. Percent myelinated area was therefore estimated based on MOG immunoreactivity above the threshold level.

Chapter III: Determination of the *in vivo* contribution of apoptosis on limited repair after chronic demyelination

Introduction/Rationale

PDGF-A is a growth factor secreted by reactive astrocytes (Redwine and Armstrong, 1998) that has the potential to act as a survival factor during OL development (Barres et al., 1992b; Gard et al., 1995; Grinspan and Franceschini, 1995). As such, the expression of PDGF-A might help regulate the survival of OL cells after demyelination, influencing the amount of apoptosis that occurs. The PDGF-A ligand is also of interest because acute experimental demyelination activates PDGFaR signaling, stimulating OL progenitor proliferation (Frost et al., 2003; Woodruff et al., 2004; Murtie et al., 2005b). Prior to the study described in this work, the PDGF-A signaling pathway had not been tested in the context of chronic demyelination (Vana et al, 2007), in which promoting OL progenitor proliferation would be beneficial for improving the repair response. Therefore, as part of an experiment to determine the effect of the PDGF-A transgene expression on the capacity of OL progenitor cells to generate mature and myelinating oligodendrocytes in chronically demyelinated lesions, apoptosis was also quantified.

More specifically, cuprizone was used to induce chronically demyelinated lesions in transgenic (tg) mice engineered to overexpress *hPDGF-A*, which is the human PDGF-A gene and is under control of the astrocytic GFAP promoter (Fruttiger et al., 2000). The control of the human transgene by GFAP reflects endogenous PDGF-A expression

because reactive astrocytes, expressing GFAP are the major source of cellular PDGF-A in demyelinated lesions (Redwine and Armstrong, 1998). In this study, mice, transgenic or wild type littermates were analyzed during both acute and chronic cuprizone demyelination as well during a recovery period on a normal chow. In addition to being a source of endogenous PDGF-A, reactive astrocytes are a potential source of several other factors that could influence OL cells (Silver and Miller, 2004; Williams et al., 2007; Gallo and Armstrong, 2008; Sofroniew and Vinters, 2010).

Materials and Methods

Mice

For this specific aim, mice were bred and maintained in the Uniformed Services University of the Health Sciences (USUHS) animal housing facility in accordance with guidelines of the National Institutes of Health and the USUHS Institutional Animal Care and Use Committee. Previous reports have characterized the *hPDGF-A* tg mouse line used for the study of this specific aim (Fruttiger et al., 2000; van Heyningen et al., 2001; Woodruff et al., 2004). Briefly, both *hPDGF-A* tg and wild-type mice were generated through in house breeding of pairs of hemizygous *hPDGF-A* tg mice brought up on a C57Bl6/cba hybrid background. Determination of the mouse genotypes were established with tail DNA PCR, which has also been described previously (Fruttiger et al., 2000). This study used heterozygous *hPDGF-A* tg mice because homozygous *hPDGF-A* tg mice exhibit deformity of the spinal cord (scoliosis) and die within the first few postnatal weeks.

In contrast, the heterozygous *hPDGF-A* tg used in this study do not have any overt CNS abnormalities. Furthermore, the *hPDGF-A* transgene used in this study is under the control of the mouse GFAP promoter (Brenner et al., 1994) and encodes a 318 bp "short" diffusible alternative-splice isoform of the human *PDGF-A* gene (Pollock and Richardson, 1992), as well as a myc epitope tag fused to the carboxy terminus. This GFAP promoter driven expression of the *hPDGF-A* transgene construct does not appear to generate any compensatory response in endogenous mouse *PDGF-A* gene expression (van Heyningen et al., 2001). Moreover, secretion of the *hPDGF-A* transgene product via the GFAP promoter has been indicated in previous studies which compared this transgene construct to a construct driven from a neuronal promoter (Fruttiger et al., 2000).

The neuronal expression of the *hPDGF-A* transgene increases OL progenitor numbers near neuron cell bodies, where PDGF-A is likely to be secreted, but does not increase OL progenitor numbers along axons which do not have a mechanism for PDGF-A secretion (Fruttiger et al., 2000). In comparison to the neuronal *hPDGF-A* construct, expression of a *hPDGF-A* transgene within the endoplasmic reticulum does not increase the OL progenitor number (van Heyningen et al., 2001). Furthermore, expression of the *hPDGF-A* transgene specifically from the GFAP promoter for astrocytes is observable in both the developing and adult CNS of hemizygous *hPDGF-A* tg mice (Fruttiger et al., 1999; Woodruff et al., 2004). Additionally, increases in *hPDGF-A* expression occur in reactive astrocytes during 6 weeks of acute cuprizone induced demyelination (Fruttiger et al., 2000; Woodruff et al., 2004).

Cuprizone Timeline

To induce demyelination, *hPDGF-A* tg mice and wt littermates were fed cuprizone as detailed previously (Chapter II, cuprizone experimental demyelination). For analysis of both acute and chronic demyelination, mice were sacrificed after 3, 6, 9, or 12 weeks on cuprizone. To assess recovery from chronic cuprizone induced demyelination, mice were continuously fed cuprizone for 12 weeks then sacrificed after being returned to normal chow for a 6 week recovery period.

In situ hybridizations

In situ hybridization was performed with methods previously detailed (Messersmith et al., 2000; Armstrong et al., 2002) using a riboprobe for PDGRαR (Redwine and Armstrong, 1998). The PDGRαR riboprobe was labeled with digoxigenin and hybridized to coronal brain sections. The digoxigenin labeling was detected with an alkaline phosphatase-conjugated sheep anti-digoxigenin antibody (Roche, Indianapolis, IN), and a subsequent reaction with NBT/BCIP substrate (DAKO, Carpinteria, CA).

Apoptosis

Apoptosis was assessed using a TUNEL assay (ApopTag in situ apoptosis detection kit; Intergen, Purchase, NY) with slight modifications. Briefly, the 3'-OH DNA ends, generated via DNA fragmentation and typically observed with in cells undergoing apoptosis, were labeled with digoxigenin-dUTP using terminal deoxynucleotidyl transferase (TdT). After labeling, the digoxigenin tagged 3'-OH DNA end were detected with an anti-digoxigenin antibody conjugated with peroxidase or fluorescein. The peroxidase labeling was detected with DAB substrate (Vector Labs, Burlingame, CA), yielding a dark brown reaction product. As a nuclei stain,

sections were also counterstained with methyl green (Vector Labs, Burlingame, CA). PDGFaR *in situ* hybridization (see above) was also performed prior to ApopTag with DAB. To identify cells at stages throughout the OL immunostaining for Olig2 (1:200; Chemicon, Temecula, CA) was performed (Ligon et al., 2006) in combination with fluorescein detection of ApopTag. For control comparisons of apoptosis in wild-type littermates of *hPDGF-A* heterozygous mice, male C57Bl/6 mice were purchased from Jackson Labs.

Quantification and statistical analysis

For analysis between categories, three or more tissue sections per mouse and three or more mice per condition were examined. The number of mice per condition is represented with "n". For comparison of cuprizone treatment effect between genotypes, an unpaired Student's *t*-test was used. A one-way analysis of variance (ANOVA) followed with a post hoc Tukey's multiple comparison was used to determine significant differences among stages of demyelination. A two-way ANOVA was used to determine the significance of mouse genotype effect across multiple treatment conditions.

Results

During recovery from chronic demyelination, apoptosis is reduced in hPDGF-A tg mice

The *in vivo* contribution of apoptosis on limited repair after chronic demyelination was determined as part of a larger study assessing the effect of the overexpression of PDGF-A in *hPDGF-A* tg mice. The aim of this over-arching study was to establish the potential of endogenous OL progenitor cells to generate mature myelinating oligodendrocytes in the context of chronic demyelination. To induce chronically demyelinated lesions, cuprizone was

used. Furthermore, after 12 weeks of continuous chronic cuprizone ingestion mice were returned to normal chow for a 6 week recovery period. During the cuprizone time-course mice were sacrificed at intervals for tissue analysis.

Overall this study demonstrates improved OL repopulation as well as remyelination in *hPDGF-A* tg mice compared to wild-type mice after recovery from chronic cuprizone ingestion (Vana et al, 2007). However, these effects are not attributable to increased OL progenitor proliferation, which was the expected mechanism, based on previous reports of the effect of PDGF-A overexpression in *hPDGF-A* tg in acute demyelination (Woodruff et al., 2004). The beneficial effect of PDGF-A overexpression on remyelination must therefore come from another cellular property rather than an effect on OL proliferation.

Survival is another cellular property that has the potential to regulate the OL progenitor response in the context of remyelination. Therefore, differences in the amount of cell death are examined using a modified TUNEL assay (Figure 1). In the absence of cuprizone treatment, low levels of TUNEL+ cells are observed in 8-week old mice of either genotype. After 3 weeks of cuprizone ingestion, similar oligodendrocyte cell loss is observed in *hPDGF-A* tg and wild-type mice (Vana et al, 2007). Correspondingly, the amount of apoptosis at 3 weeks of cuprizone treatment is analogous between mice of both genotypes (Figure 1 A, B). In contrast, after 6 weeks of acute cuprizone ingestion, the *hPDGF-A* tg mice have a larger number of TUNEL+ cells compared to the wild-type mice (Figure 1 A, B). By 12 weeks of chronic cuprizone ingestion, the amount of apoptosis is not different between mice from each genotype (Figure 1 A, B).

A representative coronal section from a wild type mouse treated with cuprizone for 12 weeks followed by a 6 week recovery period on normal chow exemplifies the CC area examined in this analysis compared to the adjacent cg (Figure 1C). TUNEL+ apoptotic cells are seen in brown and co-localize with nuclei stained with methyl green (Figure 1C inset). To identify whether oligodendrocyte lineage cells undergo apoptosis Olig2 was detected using immunohistochemistry (Figure 1D, F red). Co-labeling with TUNEL+ cells detected using a flourescin tag (Figure 1E) indicates that some apoptotic cells in the CC of cuprizone treated mice are of the oligodendrocyte cell lineage (Figure 1F). Furthermore, TUNEL+ apoptotic cells are also observed after 6 weeks of cuprizone ingestion in the mouse CC (Figure 1G, brown). PDGFaR mRNA *in situ* hybridization in that same section shows that oligodendrocyte progenitors are abundant in the mouse CC after 6 weeks of cuprizone ingestion. Moreover, there is little co-localization of TUNEL+ cells and PDGFaR *in situ* hybridization (Figure 1H), though each is observable independently at this cuprizone ingestion time-point. In contrast, during the recovery period after 12 weeks of chronic cuprizone ingestion, there is some co-labeling of TUNEL+ cells and PDGFaR *in situ* hybridization (Figure 1I).

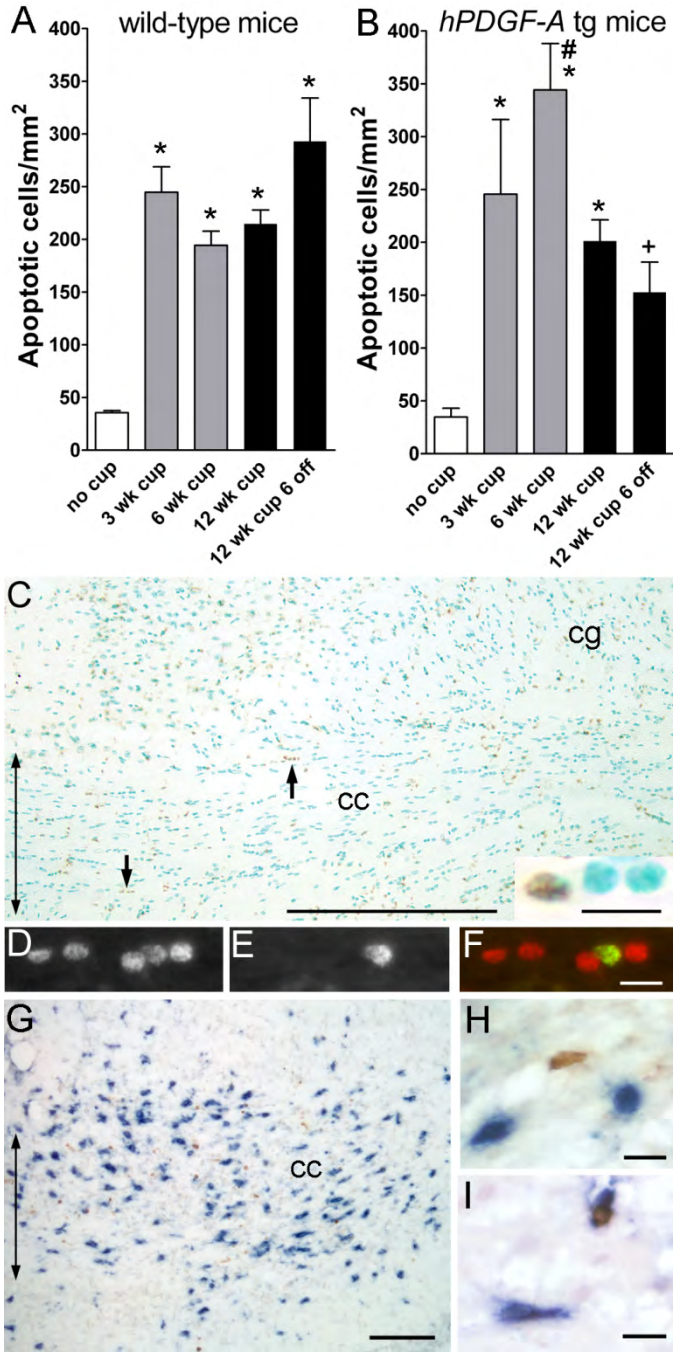
A
wild-type mice
Apoptotic cells/mm2
400
350
300
250
200
150
100
50
0
no cup
3 wk cup
6 wk cup
12 wk cup
12 wk cup 6 off
B
hPDGF-A tg mice
Apoptotic cells/mm2
no cup
3 wk cup
6 wk cup
12 wk cup
12 wk cup 6 off
C
cg
cc
D
E
F
G
cc
H
I

Figure 1. During recovery from chronic demyelination, apoptosis is reduced in hPDGF-A tg mice. A, B: Quantification of the density of apoptotic cells, identified by modified TUNEL assay, in the corpus callosum of wild-type (A) and *hPDGF-A* transgenic (tg) mice (B). White bars indicate no cuprizone treatment. Gray bars indicate perfusion after 3 or 6 weeks of cuprizone treatment. Black bars indicate perfusion after 12 weeks of continuous cuprizone feeding, or 12 weeks of cuprizone followed by 6 weeks on normal chow. During cuprizone treatment of both wild-type and *hPDGF-A* tg mice, the density of apoptotic cells is significantly increased from normal levels (***** $p < 0.05$ compared to no cup; one-way ANOVA within each genotype). With 6 weeks of cuprizone treatment, TUNEL labeling in the *hPDGF-A* tg mice is significantly increased from the wild-type mice (**#** $p < 0.05$ for *hPDGF-A* tg 6 wk cup compared to wild-type 6 wk cup; two-way ANOVA for genotype and treatment). Elevated apoptosis values continued after removal of cuprizone from the diet of wild-type mice (***** $p < 0.05$ compared to no cup). While apoptosis remains elevated somewhat during recovery in *hPDGF-A* tg mice, the values are no longer significantly above those in non-treated *hPDGF-A* tg mice. Further, apoptosis in the *hPDGF-A* tg mice is significantly decreased from the wild-type mice (**+** $p < 0.05$ for *hPDGF-A* tg 12 wk cup 6 wk off compared to wild-type 12 wk cup 6 wk off; two-way ANOVA for genotype and treatment). All statistical analyses are based on a sample size of 3-5 mice per condition. **C:** Representative coronal section showing the corpus callosum (cc, double arrow along midline; cg = cingulum) in a wild-type mouse treated with cuprizone for 12 weeks followed by a 6 week period for recovery. TUNEL (brown) signal is present in individual cells distributed throughout the corpus callosum and in groups of cells aligned as is characteristic of interfascicular oligodendrocytes (single arrows and inset). Nuclei stained with methyl green. Scale bars = 250

um and 10 um. **D-F:** Immunostaining for Olig2 (D, and red in F) to identify oligodendrocyte lineage cells in combination with TUNEL (E, and green in F) within the corpus callosum in a wild-type mouse treated with cuprizone for 12 weeks followed by a 6-week period for recovery. Scale bar for D-F shown in F is 10 um**. G-H:** Representative coronal sections showing PDGFαR mRNA *in situ* hybridization (blue/black cytoplasm) and TUNEL labeling (brown nuclei) in the corpus callosum (G: cc= corpus callosum, double arrow along cc midline). **G**: After 6 weeks of cuprizone treatment, *hPDGF-A* tg mice show OP amplification. TUNEL labeling is high but does not co-localize with PDGFaR expression, as expected for apoptosis of mature oligodendrocytes ongoing cuprizone treatment. Scale bar = 200 um. **H**, **I**: During recovery after 12 weeks of cuprizone treatment, TUNEL and PDGF*α*R mRNA transcripts can be detected separately (H; wild-type mouse) and co-localization is also observed (I; wild-type mouse). Scale bars for H and I are 10 um. Figure from (Vana et al., 2007).

After 12 weeks of continuous cuprizone ingestion, apoptosis continues during the 6-week recovery period on normal chow. During this recovery period after chronic demyelination, significantly fewer apoptotic cells were present in the corpus callosum of *hPDGF-A* tg mice compared to wild-type mice (Figure 1 A, B). The apoptotic cells identified include some cells within rows of cells aligned longitudinally between axons, which are a characteristic of interfascicular oligodendrocytes (Figure 1 C). Furthermore, Olig2 immunostaining, an indicator of immature through mature stages of the OL identifies some TUNEL+ cells (Figure 1 D-F). Additionally, some of the TUNEL+ cells express PDGFaR (Figure 1 I), indicating an OL progenitor phenotype as well as potential regulation by PDGF-A ligand levels.

These results show that apoptosis decreases after recovery from chronic demyelination in mice overexpressing PDGF-A. Furthermore, they suggest that OL cells are at least partially targeted by the continued apoptosis observed after recovery from chronic demyelination. Moreover, PDGF-A could promote cell survival during the recovery phase from chronic demyelination, which associates well with a previously suggested role for PDGF-A in the prevention of oligodendrocyte apoptosis during developmental myelination (Barres et al., 1992a).

Additional TUNEL analyses were conducted to test if the continuation of increased levels of apoptosis observed in wild-type littermates of *hPDGF-A* tg mice could be an effect of the C57Bl6/cba hybrid background. For these analyses, the TUNEL procedure was performed on C57Bl/6 mice from Jackson Laboratories, the most commonly used mouse strain for cuprizone treatment. These analyses showed that high levels of TUNEL+ cells are present in the CC of

C57Bl/6 mice during the recovery period following 12 weeks of chronic cuprizone ingestion (Vana et al 2007). Therefore, the continuation of high levels of apoptosis during recovery from chronic demyelination is not a genetic background effect and could play a part in creating the limited repair observed after chronic cuprizone induced demyelination.

Apoptosis during chronic demyelination and recovery from chronic demyelination

In this work, cuprizone demyelination increased the amount of observed apoptosis as detected by TUNEL staining (Vana et al. 2007 and Figure 1). After 12 weeks of chronic cuprizone ingestion, increases in the amount of apoptosis were still apparent and continued even after removal of cuprizone for a 6 week recovery period (Figure 1). Furthermore, the identification of some apoptotic cells as OL cells (Figure 1) indicates that OL cells can be depleted via apoptosis in this paradigm. This suggests that ongoing apoptosis in the context of chronic demyelination at least partially contributes to depletion of the OL progenitor pool, which has been reported following chronic demyelination (Armstrong et al., 2002; Mason et al., 2004; Armstrong et al., 2006; Vana et al., 2007; Xie et al., 2010). Depletion of the OL progenitor pool directly affects the capacity for remyelination, as endogenous OL progenitor cells are the major source of myelinating cells in the adult brain (Chang et al., 2002; Murtie et al., 2005b; Gallo and Armstrong, 2008; Moore et al., 2011). Moreover, these results show that apoptosis is a factor contributing to limited remyelination following chronic demyelination as apoptosis is rare after a normal chow diet (Mason et al., 2001; Armstrong et al., 2002) and Figure 1.

Additionally, supply of hPDGF-A improves cell survival by reducing apoptosis during the recovery time-period following chronic demyelination, contributing to enhanced remyelination

in corpus callosum lesions. It has been shown that during OL development PDGF-A might act as a survival factor (Barres et al., 1992b; Gard et al., 1995; Grinspan and Franceschini, 1995) and that the survival of newly generated OL cells is enhanced by the PDGF-A ligand (Barres et al., 1992b). In that model, supported by this work, it is only after maturation that new OL cells become vulnerable to the effects of cuprizone and endure apoptosis. This effect of PDGF-A on survival of new OL cells rather than mature OL cells is suggested by the fact that during acute cuprizone ingestion, there is a lack of protection for mature myelinating oligodendrocytes in *hPDGF-A* tg mice (Vana et al. 2007). Overall these results suggest that the environment generated by chronic demyelination might not give substantial support for the survival of OL cells, which could therefore contribute to the limited capacity for remyelination observed after chronic demyelination.

Importance of astrocytes in regulation of remyelination potential

Also in this work, the hPDGF-A transgene expression is under control of GFAP promoter (Fruttiger et al., 2000), which restricts overexpression to astrocytic cells (Vana et al. 2007). This selective expression of PDGF-A is meant to reflect the endogenous source of PDGF-A , which is primarily from reactive astrocytes (Redwine and Armstrong, 1998; Hinks and Franklin, 1999; Frost et al., 2003). Furthermore, a reactive astrocytic response with subsequent PDGF-A is associated with demyelinated lesions (Redwine and Armstrong, 1998; Hinks and Franklin, 1999; Fruttiger et al., 2000; Frost et al., 2003). Moreover, astrocytic overexpression of the *hPDGF* tg might correspond with appropriate ECM modulation of PDGF-A through factors like tenascin-C (Garwood et al., 2004).

Chapter IV: Characterization of the astroglial response in acute and chronic corpus callosum demyelination relative to the oligodendroglial lineage

Introduction/Rationale

The term astrogliosis has been traditionally used as an umbrella term denoting any astroglial activity. In contrast to this traditional definition of astrogliosis, many researchers now realize the need to define astrogliosis as more of a continuum of gradual changes in astrocyte morphology and phenotype expression as opposed to an all-or-none response (Sofroniew and Vinters, 2010). With this emerging definition of astrogliosis, different stages along the astroglial reactivity continuum have the potential to exert different effects on the OL response in the context of demyelination. Characterizing the extent of the astroglial response in acute and chronic demyelination should help delineate the effect that astroglial activation has on the OL response. Furthermore, astrocytes are a source of both endogenous inhibitory as well as beneficial factors toward remyelination and repair (Liberto, 2004, Sofroniew and Vinters 2010). The characterization of the extent of astrogliosis could point out factors related to astroglial activation that have the potential to influence OL cells.

Moreover, astrogliosis is described as a hallmark of many demyelinating injuries (Zhang et al., 2010; Hamby and Sofroniew, 2011; Kang and Hebert, 2011) and has been observed in several models of demyelination, including cuprizone administration (Hiremath et al., 1998; Koutsoudaki et al., 2009; Xie et al., 2010). However, the extent of astrogliosis has not been fully characterized in any of these models. Because cuprizone ingestion is not associated with a primary immune response or blood brain barrier breakdown

(Kipp et al., 2009; Kotter et al., 2011), it is good model in which to assess the influence of astroglial activation on the OL response to demyelination without additional confounding factors. Furthermore, the different time-courses of demyelination that can be mimicked with cuprizone ingestion may have different degrees of astroglial activation, leading to differential OL responses. To evaluate this possibility, the extent of astroglial activation was characterized in the CC during both acute and chronic demyelination. Characterization was completed using histopathological and immunohistochemical stains as well as real time quantitative polymerase chain reactions (RT-QPCR). The CC in particular was studied because cuprizone ingestion reliably and reproducibly demyelinates the CC in many rodent strains, including the C57bl/6 mouse strain used in this work.

Methods

Mice

Male C57BL/6 mice (6-7 weeks of age) were purchased from Jackson Laboratories (Bar Harbor, ME) and housed two per cage on a twelve hour light-dark cycle in the USUHS animal facility. Food and water were provided *ad libitum*.

Cuprizone Timeline

To induce demyelination mice were fed cuprizone as detailed previously (Chapter II, cuprizone experimental demyelination). To examine acute and chronic phases of disease progression, mice were sacrificed after 3, 6, 9, or 12 weeks on cuprizone.

To assess recovery from cuprizone induced demyelination, mice were continuously fed cuprizone for either an acute (6 week) or chronic (12 week) period then sacrificed after being

returned to normal chow for a variable recovery period of either 3 or 6 weeks on normal chow. This creates four different recovery time-points, designated 6+3 (acute demyelination, early recovery), 6+6 (acute demyelination, recovery), 12+3 (chronic demyelination, early recovery) and 12+6 (chronic demyelination, recovery).

Control mice were sacrificed at 8, 20 or 26 wks of age. These time-points were used so that control mice were age-matched to experimental cuprizone ingestion time-points. 8 weeks of age represents the earliest age mouse examined and is the starting age for cuprizone ingestion. 20 weeks of age is simultaneously a control for acute demyelination with a recovery period (6+6), as well as for chronic demyelination (12). 26 weeks of age is the oldest time-point examined and serves as a control for chronic demyelination with recovery (12+6).

Analysis of Tissue Sections

GFAP protein expression was detected using a rabbit polyclonal IgG antibody (DAKO, Carpinteria, CA) and Alexa488 secondary antibody (Invitrogen, Grand island, NY). Ki67 was detected using a modified antigen retrieval protocol. Briefly, Biogenex Antigen Retrieval Citra Solution (Biogenex, Fremont, CA) was diluted and heated in a microwave. Slides were then immersed in warm Antigen Retrieval Solution for 20 minutes at room temperature. An Alexa555 goat anti-rat secondary antibody was used for fluorescent imaging (Life Technologies, Grand island, NY). Vimentin was detected using a mouse monoclonal antibody (Millipore, MAB1681, Danvers, MA) and a donkey anti-mouse IgM secondary antibody conjugated to Cy3 (Jackson Immunoresearch, West Grove, PA). Fibronectin was detected using a rabbit anti-fibronectin antibody (Chemicon, Ab 1954, Millipore, Billerica, MA). An Alexa488 goat anti-rabbit secondary antibody (Invitrogen, Grand Island, NY) was used to visualize fibronectin staining. A

mouse monoclonal anti-chondroitin sulfate antibody (Sigma, Clone CS-56, St. Louis, MO) was used to stain for chondroitin sulfate glycoproteins (CSPG)s. To visualize the CSPG staining, a goat anti-mouse IgM secondary antibody conjugated to Cy3 (Jackson Immunoresarch, West Grove, PA) was used. For collagen staining, slides were stained using Masson's Trichrome Blue stain for collagen fibers (Histopathology core at USUHS biomedical instrumentation core, Bethesda MD).

Custom Array Analysis of Gene Expression

RNA was isolated following a modified protocol from SABiosciences (Gaithersburg, MD). At least 3 mice were processed for each experimental condition and control group. Briefly, the CC was microdissected then homogenized in TRIZOL for RNA isolation. RNA was purified using the RT^2 qPCR-Grade RNA Isolation Kit (SABiosciences, PA-001). Purity readings were determined with a Nanodrop spectrophotometer (ThermoScientific, Waltham, MA). Samples were required to have A260/280 ratios of above 2.0 and A260/230 ratios of above 1.8. If necessary, samples were re-purified according to the SABiosciences protocol.

Purified RNA samples were converted to cDNA (5 ng/10 uL) using the RT First Strand Kit (SABiosciences, C-03) for use in QPCR arrays. A custom 386-well plate was designed for expression analysis of 96 genes selected for relevance to the cuprizone remyelination and astrogliosis (SABiosciences). On each plate, four different experimental conditions were run as a set of three disease time points as well as one no cuprizone control time point. For each time point, cDNA was pooled from three mice of the same condition. Each experimental and control condition was run as technical triplicates on three different plates. Raw Ct values of 0 and above 35 were excluded from analysis as inappropriate reactions or below detection threshold

of the system. Values from four house-keeping genes (Tbp, Hprt1, Actb and 18sRNA) were used for normalization of same loading and integrity for each sample. Changes in relative mRNA fold expression across the disease time course and control ages were determined using the delta delta Ct (ΔΔCt) method; relative to the mRNA gene expression values for 8 week old mice (no cuprizone age match to 0 weeks of cuprizone treatment). GenePattern 2.0 was used to generate heatmaps of relative mRNA expression levels in each sample (Reich et al., 2006).

Statistical Analysis

Graphpad Prism 5.0 was used for graphing and statistical analyses. One-way ANOVA measures were used to determine significant differences between cuprizone treatment groups across the disease time course. Relative mRNA fold gene expression values were also each individually compared to a theoretical value of 1.0, for significance relative to no fold change, using a Students t-test. Probability values of $p < 0.05$ were considered significant.

Results

Severe diffuse astroglial activation characterizes cuprizone induced demyelination and persists during the recovery phase

To study astroglial activation during demyelination and recovery, the cuprizone model was used. It produced expected results (Armstrong et al., 2006; Vana et al., 2007; Hibbits et al., 2009) with: i) extensive demyelination in the CC after both acute and chronic cuprizone ingestion (Fig 2B, D, F), ii) spontaneous remyelination after acute cuprizone ingestion and subsequent recovery on normal chow (Fig 2C, F), and iii) limited spontaneous repair and

remyelination after chronic cuprizone ingestion and subsequent recovery on normal chow (Fig 1E, F).

During different stages of cuprizone-induced demyelination immunohistochemistry for both GFAP (Figure 3, 4) and vimentin (Figure 4), characteristic markers of reactive astrogliosis (Pekny and Nilsson, 2005; Sofroniew, 2009; Sofroniew and Vinters, 2010), was undertaken. The representative images shown (Figure 3, 4) indicate that both GFAP and vimentin are expressed during cuprizone induced demyelination as well as into the recovery period on normal chow. This suggests that astrocytes are activated by cuprizone demyelination.

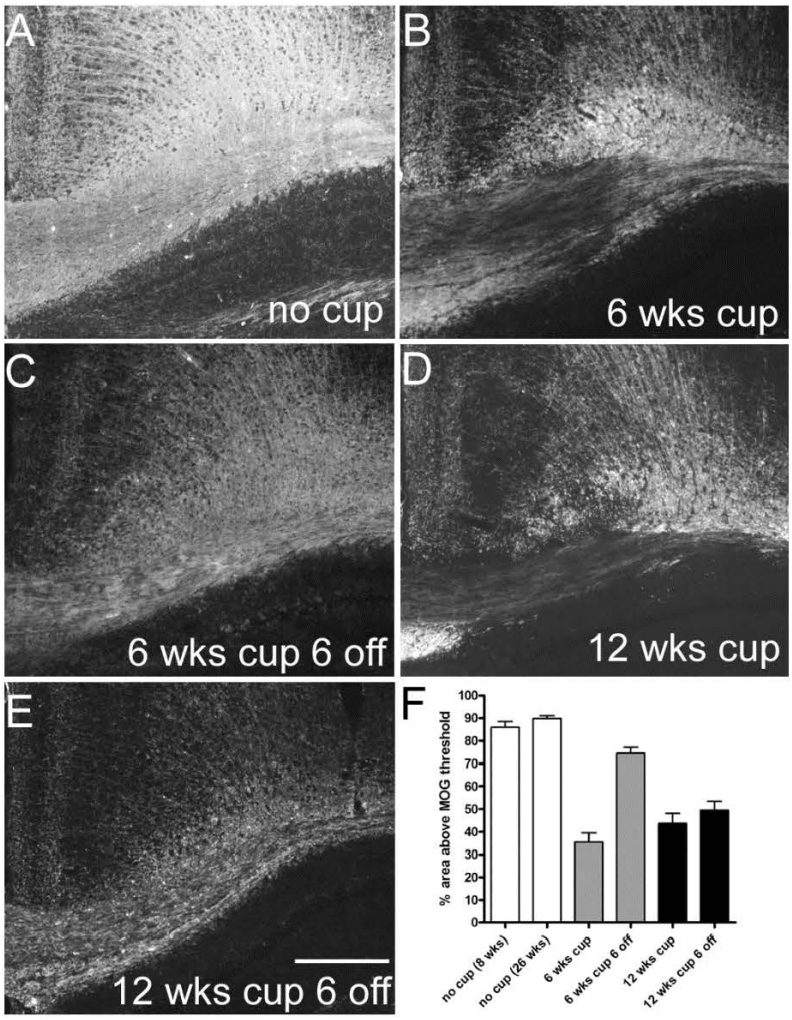
A
no cup
B
6 wks cup
C
6 wks cup 6 off
D
12 wks cup
E
12 wks cup 6 off
F
% area above MOG threshold
100
90
80
70
60
50
40
30
20
10
0
no cup (8 wks)
no cup (26 wks)
6 wks cup
6 wks cup 6 off
12 wks cup
12 wks cup 6 off

Figure 2. Representative examples of demyelination status in the mouse corpus callosum at the end-points for the cuprizone (cup) ingestion and recovery time-courses. A: No cup control mouse, 26 weeks old (age-matched to the chronic recovery time-point). **B:** 6 weeks (acute) cup ingestion shows substantial myelin loss. **C:** 6 weeks acute cup ingestion with 6 weeks of recovery on normal chow (acute recovery time-point) shows almost complete spontaneous remyelination. **D:** 12 weeks (chronic) cup ingestion shows substantial myelin loss. **E:** 12 weeks chronic cup ingestion with 6 weeks of recovery on normal chow (chronic recovery time-point) shows some spontaneous remyelination, but is not as robust as at the acute recovery time-point (**F**) Quantification of percent myelination as an indicator of demyelination status shows significant differences between cup treatment groups ($p < 0.001$); acute and chronic cup ingestion produce significant demyelination compared to no cup controls ($p < 0.001$), there is no difference between no cup treatment (8 wks or 26 wks) and the acute recovery time-point. There is still significant demyelination at the chronic recovery time-point compared to no cup ($p < 0.001$). All images processed similarly, scale bar in **E** is indicative of all images and represents 100 um.

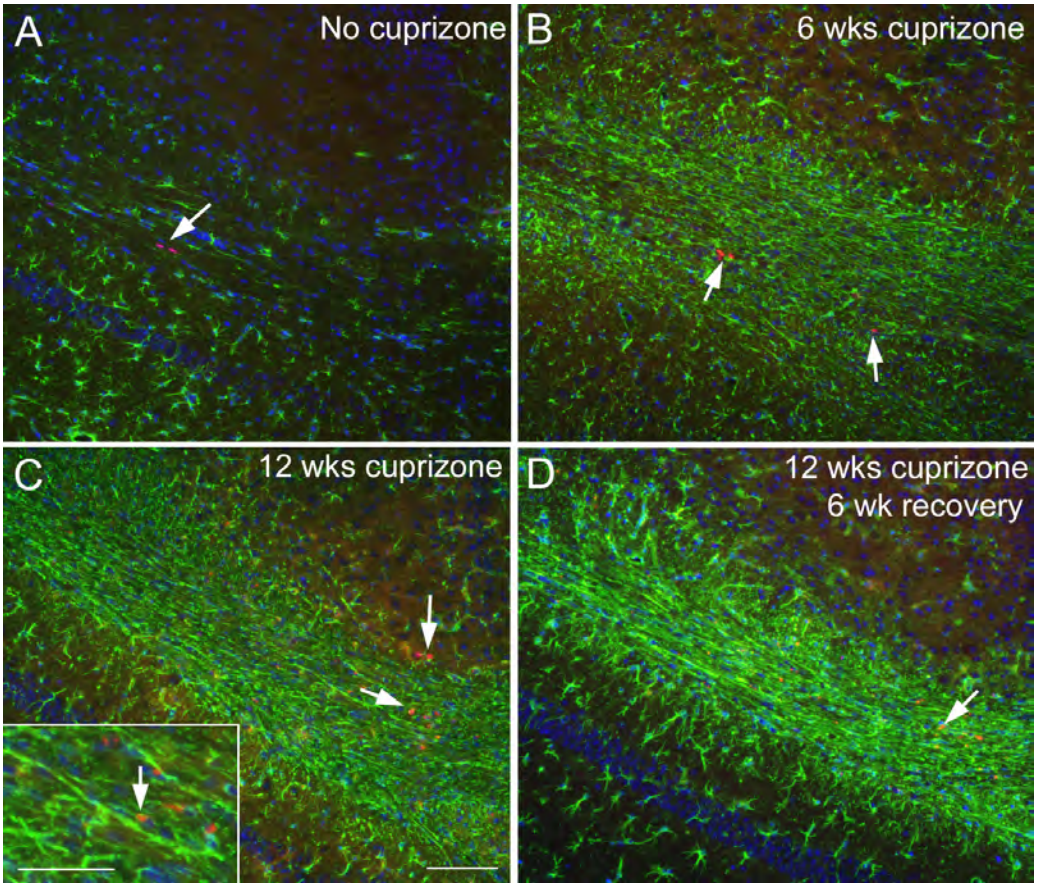

Figure 3. Proliferating and astrocytic cells are found in the corpus callosum of cuprizone treated mice, GFAP (green)/Ki67 (red)/DAPI (blue). Arrows show examples of Ki67 positive proliferating cells without cup treatment (**A**), with acute cup demyelination (6 wks cuprizone **B**), with chronic cup demyelination (12 wks cuprizone **C**) and in recovery after chronic demyelination (12 wks cuprizone, 6 wk recovery **D**). Co-immunostaining of GFAP and Ki67 is indicative of proliferative astrogliosis in this model of demyelination. Scale bar in (C) 12 wks cuprizone is characteristic of all images in the panel and represents 100 um. The scale bar on the inset in (C) 12 wks cuprizone represents 50 um.

Furthermore, Ki67 co-localization with GFAP (Figure 3) shows that astrocytes are proliferating in this model of demyelination. Astrocytic proliferation is characteristic of severe diffuse astrogliosis as opposed to the less activated stage of mild to moderate astrogliosis, since there is very little proliferation in mild to moderate astrogliosis (Sofroniew and Vinters, 2010). Therefore, astrogliosis in the cuprizone model is at least at the stage of severe diffuse reactive astrogliosis. This characterization is further supported by cellular hypertrophy and some loss of cellular domains (Sofroniew and Vinters, 2010) that is apparent in GFAP expressing astrocytes after cuprizone ingestion (Figure 3).

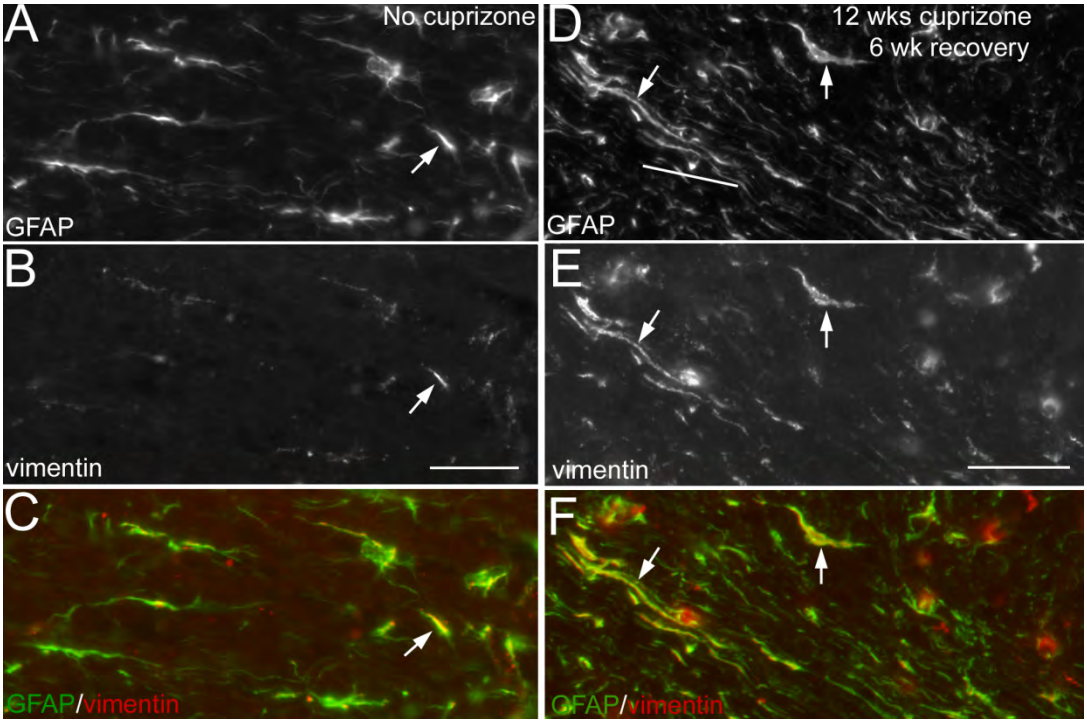

Figure 4. Reactive astrocyte immunostaining is evident into the recovery period after chronic cuprizone ingestion(12 wks cuprizone, 6 wk recovery) in the mouse corpus callosum with GFAP (**D**), vimentin (**E**) and GFAP (green)/Vimentin (red) co-localized (**F**, arrows) immunoreactivity compared to control (no cuprizone) GFAP (**A**), vimentin (**B**) and GFAP (green)/Vimentin (red) co-localized (**C**, arrow) immunoreactivity. Scale bars represent 50 um for all images in panel.

Astrogliosis in the cuprizone model does not reach the point of glial scar formation

To distinguish the extent of astrogliosis in the cuprizone model, that is whether astrogliosis reaches the most extreme end of the astrocytic continuum, designated severe diffuse astrogliosis with compact glial scarring (Sofroniew and Vinters, 2010), staining for CSPG (Figure 5), fibronectin (Figure 6) and collagen (Figure 7) were conducted. CSPGs, fibronectin and collagen are components of the ECM that is characteristic of fibrotic scarring (Schwab and Bartholdi, 1996). Fibrotic scarring characterizes CNS trauma (Yoshioka et al., 2010) and coincides temporally and spatially with astrocytic activation (Klapka and Muller, 2006). Additionally, astrocytes are influenced by ECM molecules both through the production of and interaction with ECM components (Eddleston and Mucke, 1993). Moreover, though scarring, composed of both a glial and fibrotic component, has long been considered an impediment to regrowth and repair (Sofroniew, 2009), there are many different components of the ECM and not all of them are inhibitory toward regrowth and repair.

Furthermore, the CSPGs alone constitute a diverse set of proteins that can both inhibit and promote growth (Haylock-Jacobs et al., 2011). Moreover, even inhibitory CSPGs which constitute a chemical barrier to re-growth and repair do not form a physical barrier for growth and repair (Hsu, 2006, Davies 1997). Figure 5 shows that generalized CSPG staining is present into the recovery period from chronic cuprizone administration in the mouse CC, indicating the presence of the beginning stages of a glial scar.

Fibronectin is a fibrous protein that is beneficial for cell migration, synapse formation and neurite outgrowth (Schwab and Bartholdi, 1996; Tate et al., 2007; Tucker and Mearow, 2008).

Fibronectin, since it can bind collagen, may act as a scaffold for ultimate scar formation. Indeed, collagen fibrils fail to accumulate in the absence of a fibronectin matrix (Singh et al., 2010). Figure 6 shows that fibronectin is characteristic in the mouse CC after cuprizone induced demyelination. This further indicates that the beginnings of a glial scar are present in the cuprizone model of demyelination. The glial scar is composed of several different cellular components including reactive astrocytes, microglia cells, basal membrane components and endothelial cells. Each of these components contributes to factors affecting growth and re-growth in the CNS. However, collagen, a possible source of the ultimate physical barrier toward regrowth and remyelination (Schwab and Bartholdi, 1996; Buss et al., 2007) is not present in the CC of cuprizone treated mice (Figure 7). Taken together, these results indicate that during cuprizone administration astrogliosis reaches the point of severe diffuse reactive astrogliosis without formation of a compact glial scar.

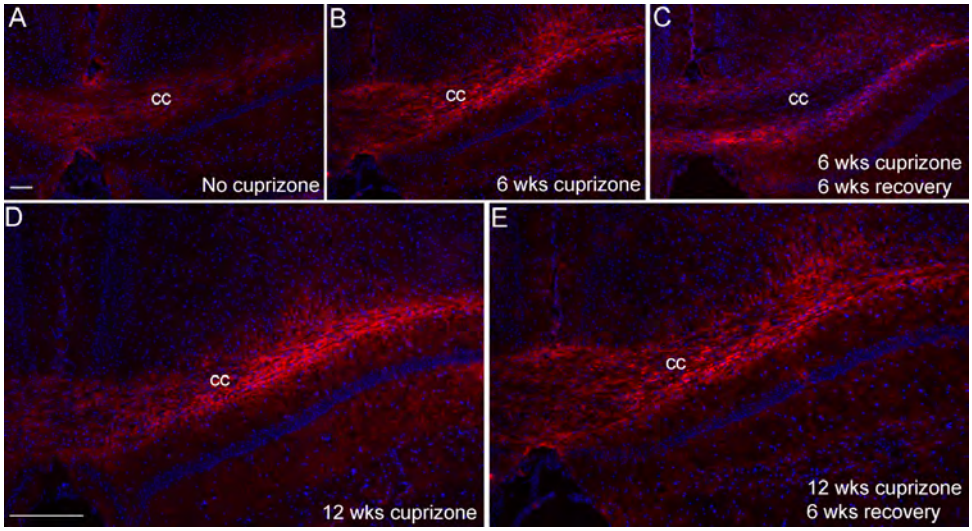

Figure 5. CSPG immunostaining (red)/DAPI nuclear staining (blue) is evident in the mouse corpus callosum at all stages of cuprizone ingestion. (A) No cuprizone control mouse, (**B**) acute cuprizone ingestion (6 wks cuprizone), (C) acute recovery cuprizone time-course (6 wks cuprizone and 6 wks recovery on normal chow), (D) Chronic cuprizone ingestion (12 wks cuprizone) and (E) chronic recovery cuprizone time-course (12 wks cuprizone and 6 wks reverie on normal chow). Scale bar for images A-C is shown in (A) No cuprizone and represents 100 um. Scale bar for images D-E is shown in (D) 12 wks cuprizone and represents 200 um.

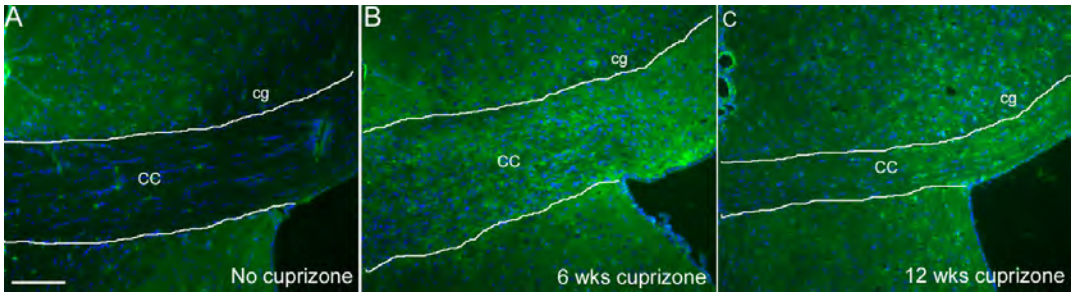

Figure 6. **Fibronectin immunostaining (green)/DAPI nuclear staining (blue)** is evident in the mouse corpus callosum (CC) after both acute (6 wks cuprizone, **B**) and chronic cuprizone (12 wks cuprizone, **C**) compared to control (no cuprizone, **A**). CC area is differentiated (white lines) from the apex of the cingulum (cg). Scale bar in (A) No cuprizone is indicative of all images in panel and represents 100 um.

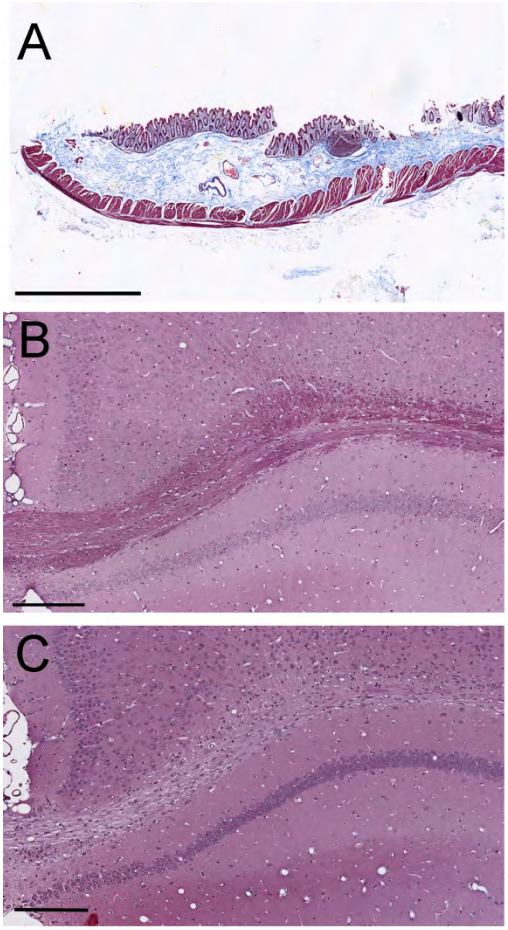

Figure 7. **Collagen, one component of glial scarring, is not present in the corpus callosal area of the brain in cup treated mice.** Masson trichrome stain for collagen turns blue in the presence of collagen and is apparent in an intestinal control section (**A)**, but not in the corpus callosum of mice treated with cuprizone to induce acute (**B**) or chronic (**C**) demyelination. Scale bar in (A) represents 2 mm, in (B) and (C) represents 200 um.

Cuprizone demyelination corresponds with increased relative mRNA expression of a constellation of genes potentially related to astroglial activation

To further characterize the extent of astrogliosis and the factors that related to astrogliosis in the cuprizone model of demyelination, a custom 386 well mRNA microarray plate was used. A total 66 genes were within threshold values for analysis (Figure 8). Of these genes, 22 cluster with GFAP, indicating that they have the same relative mRNA expression profile as GFAP in the mouse CC during both acute and chronic cuprizone ingestion and recovery (Figure 8 to arrow). The mRNA expression profile of GFAP constitutes increases in relative fold-change throughout the cuprizone ingestion time-course (Table 1, row 1, Table 2, row 2), which is expected according to the GFAP immunohistochemistry (Figure 3). Furthermore, genes that were expected to decrease during cuprizone administration, such as PLP, a myelin related gene, do not cluster with GFAP (Figure 8). These genes show a pattern of decreases in relative fold mRNA expression levels during cuprizone administration (Figure 8) when the expression of mature myelin-related genes has been shown to be maximally depleted (Matsushima and Morell, 2001; Armstrong et al., 2002). These results exemplify the fidelity of the clustering algorithm in detecting mRNA expression patterns.

The relative mRNA expression profile of genes in the GFAP cluster indicates that the transcription of genes within the GFAP cluster is most prominent during the first few weeks of cuprizone demyelination (Table 1, 2). During this early demyelination period the population of oligodendrocyte progenitor cells amplifies in the CC (Matsushima and Morell, 2001; Armstrong et al., 2006). The mRNA gene expression profile of GFAP also indicates that the gene expression

within the GFAP cluster is decreased during recovery on normal chow (Figure 8). In fact, the relative mRNA expression values within the GFAP cluster begin to decrease after initial cuprizone administration in both the acute recovery (Table 1) and chronic recovery (Table 2) cuprizone ingestion time-lines. This indicates that gene regulation of astroglial activity occurs early in the cuprizone model.

Moreover, initial astroglial activation does not appear to inhibit the OL response to demyelination as the initial astroglial activation coincides with OL progenitor amplification in the cuprizone-induced lesion area (Murtie et al., 2005b). The OL progenitor amplification during cuprizone ingestion subsequently leads to robust remyelination which can be observed during the recovery period after acute cuprizone demyelination (Figure 2C, F). Astrogliosis at this same time-point does not appear to inhibit that OL response in any form.

TABLE 1
Quantitative RT-PCR of cell type markers and signaling components clustered with GFAP for the acute recovery time-course

Gene	0 wk No cup	3 wk cup	6 wk cup	6 wk cup 3 wk off	6 wk cup 6 wk off	20 wk No cup	ANOVA p Value
Gfap	**1** ±0.02461	**14.02*** ±0.8744	**7.638*** ±0.6154	**3.316*** ±0.0935	**2.956*** ±0.386	**0.7943** ±0.116	**P<0.0001**
Vim	**1** ±0.1063	**14.7*** ±0.2464	**6.682*** ±0.1363	**3.393*** ±0.09534	**3.16*** ±0.3243	**1.201** ±0.1325	**P<0.0001**
Tnfrs1b	**1** ±0.185	**8.87*** ±0.2393	**3.877*** ±0.2187	**1.656** ±0.4516	**2.14** ±0.3657	**1.377*** ±0.03391	**P<0.0001**
Ltbr	**1** ±0.03837	**3.222*** ±0.1151	**2.097*** ±0.1764	**1.231*** ±0.04725	**1.676** ±0.1626	**1.017** ±0.07668	**P<0.0001**
Fgf2	**1** ±0.04397	**5.162*** ±0.2075	**4.009*** ±0.3605	**2.454*** ±0.1874	**2.112*** ±0.2125	**1.347*** ±0.04386	**P<0.0001**
Tnfrs1a	**1** ±0.06373	**5.97*** ±0.3629	**3.719*** ±0.1785	**1.862** ±0.4582	**1.643** ±0.187	**1.147** ±0.1593	**P<0.0001**
Tnc	**1** ±0.1445	**2.036** ±0.2725	**1.517** ±0.238	**0.839*** ±0.0287	**0.888** ±0.0322	**0.521*** ±0.0467	**0.0003**
Tgfb1	**1** ±0.07887	**5.591*** ±0.1422	**2.483*** ±0.2637	**1.542*** ±0.09363	**1.777** ±0.196	**1.11** ±0.0383	**P<0.0001**
Tgfbr1	**1** ±0.05794	**6.07*** ±0.195	**2.212*** ±0.09753	**1.511** ±0.2079	**1.373** ±0.1669	**0.9299** ±0.03499	**P<0.0001**
Axl	**1** ±0.02217	**6.453*** ±0.646	**2.355*** ±0.1454	**1.602*** ±0.05643	**1.7** ±0.174	**1.333** ±0.1293	**P<0.0001**
Itgam	**1** ±0.08201	**4.921*** ±0.2696	**2.028*** ±0.1678	**1.572*** ±0.0352	**1.2** ±0.299	**1.051** ±0.05668	**P<0.0001**
Il1b	**1** ±0.0832	**10.08*** ±0.5758	**3.134*** ±0.4724	**1.544** ±0.148	**2.268*** ±0.2327	**1.645*** ±0.02308	**P<0.0001**

Tgfbr2	**1** ±0.1841	**4.939*** ±0.3326	**1.913** ±0.3169	**1.396*** ±0.05873	**1.894*** ±0.1181	**1.11*** ±0.02265	**P<0.0001**
Bmp4	**1** ±0.2344	**3.65*** ±0.06119	**1.365** ±0.1214	**1.029** ±0.1317	**1.11** ±0.1333	**0.8315** ±0.07878	**P<0.0001**
Tnf	**1** ±0.2868	**22.8*** ±3.616	**5.969*** ±0.6915	**4.07** ±1.658	**3.198** ±0.7704	**3.652** ±0.767	**P<0.0001**
Igf1	**1** ±0.09595	**6.058*** ±0.8729	**3.259*** ±0.7182	**1.376*** ±0.06721	**2.089** ±0.6542	**1.680** ±0.4154	**P<0.0001**
Nes	**1** ±0.04636	**2.712*** ±0.06519	**1.954** ±0.2471	**1.014** ±0.05239	**1.099** ±0.2559	**1.109*** ±0.02112	**P<0.0001**
Fn1	**1** ±0.03999	**3.26*** ±0.1252	**1.776** ±0.3422	**0.9646** ±0.02701	**1.38** ±0.1125	**1.591*** ±0.04706	**P<0.0001**
Ntrk2	**1** ±0.05003	**2.062*** ±0.09052	**1.599*** ±0.0256	**1.359** ±0.1266	**1.468*** ±0.1063	**1.294*** ±0.02614	**P<0.0001**
Ptprz1	**1** ±0.02475	**2.316*** ±0.1197	**1.907*** ±0.1853	**1.562*** ±0.05879	**1.873*** ±0.1324	**1.172** ±0.07001	**P<0.0001**
Lif	**1** ±0.2182	**3.33** ±0.8421	**2.956*** ±0.15	**1.696** ±0.3317	**1.924*** ±0.1709	**1.44** ±0.3026	**0.0118**
Sox9	**1** ±0.05576	**1.616*** ±0.05583	**1.409** ±0.1583	**1.185*** ±0.02617	**1.545** ±0.1407	**1.157** ±0.06305	**0.0043**

Values shown are fold change (mean ± s.e.m.) calculated relative to 0 wk No cuprizone condition. N = 3 mice per condition with samples run across 3 plates as technical triplicates. ANOVA values are for comparison across all time points for a given gene. Asterisks show significant changes ($p < 0.05$) for individual time points using a one sample t-test comparison to a theoretical mean of 1.000, i.e. null hypothesis for no fold change.

TABLE 2
Quantitative RT-PCR of cell type markers and signaling components clustered with GFAP for the chronic recovery time-course

Gene	0 wk No cup	3 wk cup	6 wk cup	9 wk cup	12 wk cup	12 wk cup 3 off	12 wk cup 6 off	26 wk No cup	ANOVA p Value
Gfap	**1** ±0.0246	**14.02*** ±0.8744	**7.638*** ±0.6154	**5.006*** ±0.7865	**6.35*** ±0.1658	**3.111*** ±0.2658	**1.299*** ±0.01078	**0.9806** ±0.08831	**<0.0001**
Fgf2	**1** ±0.0440	**5.162*** ±0.2075	**4.009*** ±0.3605	**2.631*** ±0.072	**3.282*** ±0.062	**2.037*** ±0.1915	**1.332** ±0.1032	**1.124** ±0.1654	**<0.0001**
Igf1	**1** ±0.0960	**6.058*** ±0.504	**3.259*** ±0.415	**1.681*** ±0.050	**2.579*** ±0.176	**1.5** ±0.2337	**0.8174** ±0.2308	**1.001** ±0.0380	**<0.0001**
Tnfrs1a	**1** ±0.0637	**5.97*** ±0.3629	**3.719*** ±0.179	**2.367*** ±0.171	**2.398** ±0.380	**1.712** ±0.429	**1.488** ±0.186	**0.8077** ±0.2244	**<0.0001**
Il1b	**1** ±0.0832	**10.08*** ±0.5758	**3.134*** ±0.472	**3.781*** ±0.627	**2.898*** ±0.1719	**1.325** ±0.4113	**1.517** ±0.1649	**1.013** ±0.1739	**<0.0001**
Tnf	**1** ±0.2868	**22.8*** ±3.620	**5.969*** ±0.692	**12.33*** ±1.075	**8.11** ±1.872	**4.684** ±1.179	**3.253** ±1.372	**1.639** ±0.3837	**<0.0001**
Nes	**1** ±0.0464	**2.712*** ±0.0652	**1.954** ±0.247	**1.99** ±0.243	**1.499** ±0.1734	**1.432** ±0.1205	**0.944** ±0.1209	**0.8035*** ±0.0340	**0.0002**
Tnc	**1** ±0.1445	**2.036** ±0.2725	**1.517** ±0.238	**1.813*** ±0.094	**1.482** ±0.129	**0.789*** ±0.0236	**0.621*** ±0.05807	**0.441*** ±0.0232	**0.002**
Vim	**1** ±0.1063	**14.7*** ±0.2464	**6.682*** ±0.136	**5.14*** ±0.688	**4.003*** ±0.2476	**3.168*** ±0.08056	**1.631** ±0.1496	**1.082** ±0.0539	**<0.0001**
Tnfrs1b	**1** ±0.185	**8.87*** ±0.2393	**3.877*** ±0.219	**3.267*** ±0.238	**2.7** ±0.4865	**1.684** ±0.3582	**1.717** ±0.1867	**1.198** ±0.0799	**<0.0001**

Tgfb1	**1** ±0.07887	**5.591*** ±0.1422	**2.483*** ±0.264	**2.171*** ±0.151	**1.893*** ±0.201	**2.155*** ±0.0999	**1.364** ±0.2022	**0.9822** ±0.0776	**<0.0001**
Itgam	**1** ±0.08201	**4.921*** ±0.2696	**2.028*** ±0.168	**1.478*** ±0.065	**1.489*** ±0.0401	**1.274** ±0.1573	**1.166*** ±0.0282	**1.003** ±0.0481	**<0.0001**
Tgfbr1	**1** ±0.0579	**6.07*** ±0.195	**2.212*** ±0.098	**1.499** ±0.173	**1.43*** ±0.0417	**1.15** ±0.0478	**1.411** ±0.0995	**1.129** ±0.1087	**<0.0001**
Axl	**1** ±0.0222	**6.453*** ±0.646	**2.355*** ±0.145	**1.874*** ±0.087	**1.459*** ±0.057	**1.998** ±0.307	**1.373** ±0.0937	**1.061** ±0.0774	**<0.0001**
Fn1	**1** ±0.0399	**3.26*** ±0.125	**1.776** ±0.342	**1.133*** ±0.030	**1.078** ±0.0298	**1.166** ±0.0791	**0.912** ±0.0812	**0.8629*** ±0.0276	**<0.0001**
Bmp4	**1** ±0.2344	**3.65*** ±0.0612	**1.365** ±0.121	**0.9548** ±0.144	**0.924*** ±0.001	**1.114** ±0.1005	**0.9338** ±0.1162	**0.7667*** ±0.0321	**<0.0001**
Tgfbr2	**1** ±0.1841	**4.939*** ±0.3326	**1.913** ±0.317	**1.346** ±0.232	**1.723*** ±0.133	**1.932*** ±0.1002	**1.613** ±0.1472	**1.26*** ±0.0499	**<0.0001**
Ltbr	**1** ±0.0384	**3.222*** ±0.1151	**2.097*** ±0.176	**1.345*** ±0.054	**1.683*** ±0.116	**1.965*** ±0.125	**1.376*** ±0.0802	**1.067** ±0.146	**<0.0001**
Ntrk2	**1** ±0.0500	**2.062*** ±0.0905	**1.599*** ±0.026	**1.307*** ±0.050	**1.693*** ±0.076	**1.647*** ±0.1113	**1.307*** 0.0553	**1.048** ±0.0674	**<0.0001**
Ptprz1	**1** ±0.0248	**2.316*** ±0.1197	**1.907*** ±0.185	**1.355*** ±0.077	**1.505** ±0.171	**1.675*** ±0.0442	**1.273** ±0.223	**1.082** ±0.0522	**0.0001**
Sox9	**1** ±0.05576	**1.616*** ±0.0558	**1.409** ±0.1583	**1.64*** ±0.0882	**1.13** ±0.142	**1.829*** ±0.1421	**0.8482** ±0.1363	**0.9358** ±0.0169	**0.0018**
Lif	**1** ±0.2182	**3.33** ±0.8421	**2.956*** ±0.150	**2.10** ±0.6455	**1.527** ±0.473	**1.543** ±0.3723	**1.37** ±0.302	**1.294** ±0.1324	**0.048**

Values shown are fold change (mean ± s.e.m.) calculated relative to 0 wk No cuprizone condition. N = 3 mice per condition with samples run across 3 plates as technical triplicates. ANOVA values are for comparison across all time points for a given gene. Asterisks show significant changes ($p < 0.05$) for individual time points using a one sample t-test comparison to a theoretical mean of 1.000, i.e. null hypothesis for no fold change.

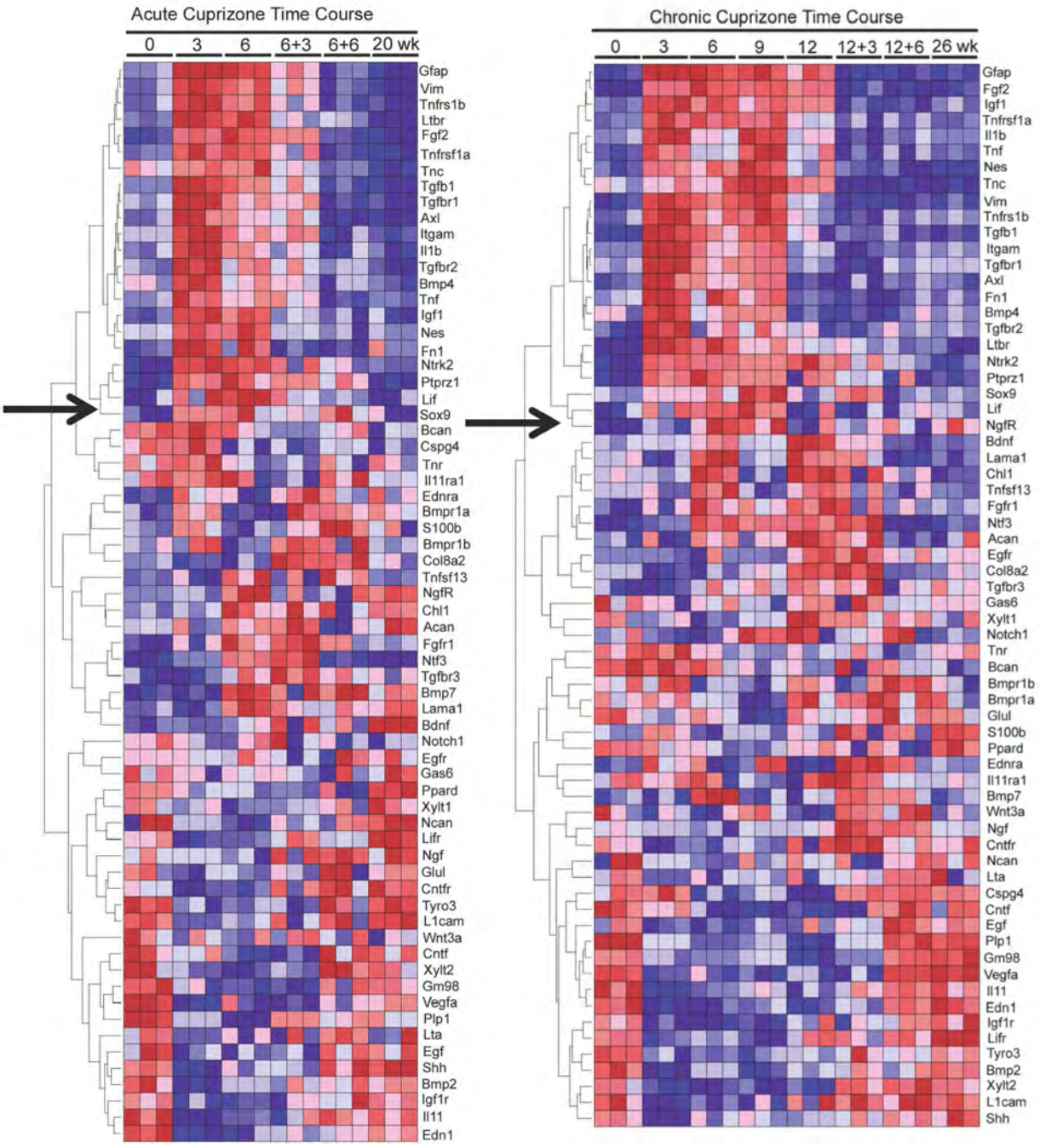
Acute Cuprizone Time Course
0
3
6
6+3
6+6
20 wk
Gfap
Vim
Tnfrs1b
Ltbr
Fgf2
Tnfrsf1a
Tnc
Tgfb1
Tgfbr1
Axl
Itgam
Il1b
Tgfbr2
Bmp4
Tnf
Igf1
Nes
Fn1
Ntrk2
Ptprz1
Lif
Sox9
Bcan
Cspg4
Tnr
Il11ra1
Ednra
Bmpr1a
S100b
Bmpr1b
Col8a2
Tnfsf13
NgfR
Chl1
Acan
Fgfr1
Ntf3
Tgfbr3
Bmp7
Lama1
Bdnf
Notch1
Egfr
Gas6
Ppard
Xylt1
Ncan
Lifr
Ngf
Glul
Cntfr
Tyro3
L1cam
Wnt3a
Cntf
Xylt2
Gm98
Vegfa
Plp1
Lta
Egf
Shh
Bmp2
Igf1r
Il11
Edn1
Chronic Cuprizone Time Course
0
3
6
9
12
12+3
12+6
26 wk
Gfap
Fgf2
Igf1
Tnfrsf1a
Il1b
Tnf
Nes
Tnc
Vim
Tnfrs1b
Tgfb1
Itgam
Tgfbr1
Axl
Fn1
Bmp4
Tgfbr2
Ltbr
Ntrk2
Ptprz1
Sox9
Lif
NgfR
Bdnf
Lama1
Chl1
Tnfsf13
Fgfr1
Ntf3
Acan
Egfr
Col8a2
Tgfbr3
Gas6
Xylt1
Notch1
Tnr
Bcan
Bmpr1b
Bmpr1a
Glul
S100b
Ppard
Ednra
Il11ra1
Bmp7
Wnt3a
Ngf
Cntfr
Ncan
Lta
Cspg4
Cntf
Egf
Plp1
Gm98
Vegfa
Il11
Edn1
Igf1r
Lifr
Tyro3
Bmp2
Xylt2
L1cam
Shh

Figure 8. **The relative mRNA expression profile of GFAP, an astrocyte marker, defines an expression profile that might characterize astrocytic signaling in cuprizone demyelination.** Hierarchical clustering of genes based on their similarity to GFAP relative fold mRNA expression distinguishes a similar gene cluster in the acute (left) and chronic (right) cuprizone treatment and recovery time-courses. The colors of the heatmap range from darkest blue (lowest relative mRNA expression) to darkest red (highest relative mRNA expression). The dendrograms represent hierarchical clusters according to similarity to GFAP relative mRNA expression, with mRNA gene expression profiles most similar to the GFAP mRNA gene expression at the top of the figure. The arrow on the left of each dendrogram depicts the end of the cluster of genes with an mRNA expression profile most similar to GFAP. The heatmap colors for each gene represent fold relative mRNA expression compared to no cuprizone (0 wk) treatment. The three technical replicates are shown for each time-point.

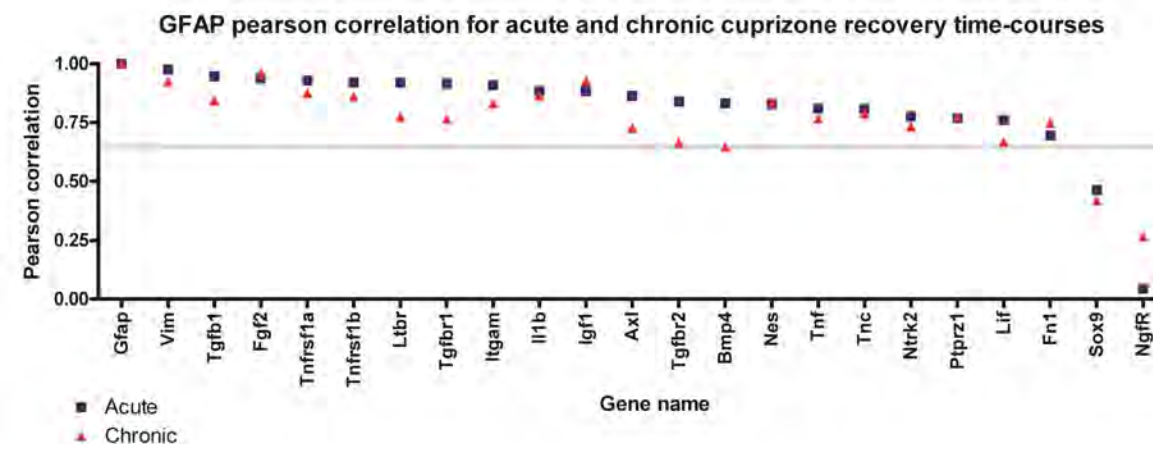

Figure 9. Scatterplot representation of genes within the GFAP hierarchical cluster for acute (blue squares) and chronic (red triangles) cuprizone ingestion time-courses. Gene names are listed along the x-axis. The number represents the Pearson correlation coefficient for the similarity of that particular gene relative mRNA expression profile to the GFAP relative mRNA expression profile for that time-course. The gray line at 0.65 represents a cut-off for strong correlation profiles to the relative mRNA expression profile of GFAP.

Furthermore, the identification of a specific set of genes within the GFAP cluster suggests a constellation of genes related to astroglial activation. Though the specificity of the indicated gene constellation for characterizing the degree of astroglial activity is as yet unknown, the results presented show that the same group of genes delineates astroglial activation in both the acute and chronic recovery time-courses of cuprizone demyelination. The extent of astroglial activity in both these cuprizone ingestion time-courses likely occurs to the same degree, termed severe diffuse reactive astrogliosis without compact glial scarring (Sofroniew and Vinters 2010, Figures 2-7). The custom gene microarray analysis with RT-QPCR of cuprizone ingestion time-courses conducted in this work further supports this characterization of the extent of astroglial activation.

The quantification of relative mRNA expression indirectly correlates with protein level expression, as genes must first be transcribed via mRNA transcripts before proteins are expressed. The temporal relationship between gene transcription and protein expression varies between genes (Yosef and Regev, 2011). Therefore, validation of protein expression is necessary to interpret the functional meaning of changes in relative fold mRNA expression. In this work, the expression of several proteins indicated on the custom microarray as potentially being involved with astroglial activation is validated using immunohistochemistry. First, the relative increase in the mRNA expression profile of GFAP throughout the course of cuprizone (Table 1, 2, row 1) corresponds with GFAP immunostaining throughout the cuprizone ingestion time-course (Figure 3). This shows that increases in GFAP mRNA relative fold expression

induced by cuprizone ingestion results in GFAP protein expression throughout the cuprizone ingestion time-course.

Second, relative increases in fold mRNA expression levels of vimentin also occur throughout the cuprizone ingestion time-course, except at the chronic recovery time-point (Table 2, row 9). Despite lack of increases in relative mRNA expression for vimentin at the chronic recovery time-period, immunostaining for vimentin is evident at this time-point compared to control tissue (Figure 4). This suggests that vimentin protein levels remain elevated throughout the course of cuprizone ingestion, even though active vimentin mRNA transcription may cease upon removal of cuprizone from the diet.

Third, immunostaining for CSPG proteins shows that there CSPG expression persists into the recovery period after chronic cuprizone ingestion in the CC of mice throughout the cuprizone ingestion time-course (Figure 5). Correspondingly, ptprz1 relative mRNA gene expression shows increases throughout the cuprizone ingestion time-course, except at 12 weeks chronic demyelination (Table 1, row 20, Table 2, row 20). Ptprz1 codes for phosphacan, a growth-inhibitory CSPG that can be secreted by astrocytes. Therefore, the relative increases of ptprz1 mRNA expression (Table 1, row 20, Table 2, row 20) could partially explain the observed CSPG immunostaining (Figure 5), as increased phosphacan mRNA transcription and subsequent phosphacan protein expression would be expected to be detected with CSPG immunostaining.

Fourth, the relative mRNA expression of fibronectin (Fn1) increases only at 3 weeks cuprizone ingestion (Table 1, row 18, Table 2, row 15) and at 9 weeks of cuprizone ingestion (Table 2, row 15), whereas fibronectin immunostaining is evident at both acute (6) and chronic

(12) cuprizone ingestion time-points (Figure 6). This suggests a delayed temporal relationship between increases in relative mRNA expression and subsequent protein expression for fibronectin, such that significant increases in fold mRNA transcription levels as observed at 3 weeks of cuprizone ingestion for fibronectin, is indirectly evident via observable fibronectin protein immunostaining 3 weeks later at the acute cuprizone demyelination time-point. Additionally, the fibronectin immunostaining observed after chronic (12) cuprizone ingestion (Figure 6) could reflect both persistent fibronectin protein expression after initial (3 week cuprizone) mRNA relative fold expression level increases (Table1, row 18, Table 2, row 15), as well as additional fibronectin protein expression resulting from significant increases of relative fibronectin mRNA fold expression levels after 9 weeks of cuprizone ingestion (Table 2, row 15).

Fifth, lack of collagen staining even after chronic cuprizone demyelination, is not only apparent with histopathological staining (Figure 7), but is reflected in the custom gene array analysis as well. Since the relative mRNA expression pattern of col8a2, the gene encoding a collagen variant, does not cluster with GFAP mRNA expression profile for astrocytic-related genes (Figure 8), collagen expression is not expected to correlate with astroglial activation in cuprizone induced demyelination. Though col8a2 relative mRNA expression changes through the course of cuprizone ingestion (Figure 8), the relative mRNA expression level change is only significantly different from control mRNA expression of col8a2 at the 6+3, 6+6, 12 and 12+3 cuprizone ingestion time-points. Furthermore, the magnitude of the relative mRNA expression of col8a2 at the time-points indicated (2.17 +/- 0.22 for 6+3, 2.51 +/- 0.08 for 6+6, 2.24 +/- 0.12 for 12, 3.34 +/- 0.22 for 12+3) is modest, suggesting little eventual change in protein expression levels, which is observed (Figure 7).

Taken together these observations show the validity of characterizing astrogliosis with RT-QPCR techniques in the cuprizone model. Furthermore, the relative mRNA expression levels observed correspond with the observed expression of various proteins and also the specific clustering of genes as following the GFAP relative mRNA expression profile suggests that the extent of astroglial activity during cuprizone demyelination can be characterized as severe reactive astrogliosis without compact glial scar formation. Using GFAP clustering to indicate a constellation of astroglial-related genes (Figure 8) not only validates the expression of known astroglial-related genes, such as GFAP and vimentin, but also points out the potential importance of other genes, such as FGF2 and tenascin-C (Tnc) whose relationship to astroglial activation are less well characterized. Moreover, identification of such genes demonstrates a potential avenue for regulation of the OL response to demyelination, as both FGF2 (Armstrong et al., 2002; Murtie et al., 2005a; Zhou et al., 2006) and tenascin-C (Gutowski et al., 1999; Holley et al., 2003; Garwood et al., 2004) have been shown to affect OL cell differentiation with a possible role in the context of MS lesions.

To further expand on this point, Figure 9 shows the Pearson correlation coefficient for the relative mRNA expression profile of each gene to its respective GFAP relative mRNA expression profile. That is, each dot on the graph represents to correlation of that gene's relative mRNA expression profile to the GFAP relative mRNA expression profile within that particular time-course (Figure 9). The only two genes whose relative mRNA expression profile does not have a strong correlation with GFAP are Sox9 and NgfR (Figure 9). Both these genes are the last row of either the acute (Sox9) or chronic (NgfR) cuprizone ingestion recovery time-courses. This

suggests that the clustering algorithm is viable and efficiently selected genes most closely resembling the expression profile of GFAP relative mRNA expression.

In addition to further validating the fidelity of the clustering algorithm, Figure 9 also points out two types of relationships for genes within the GFAP cluster. First, there are genes that have nearly the same correlation coefficient for both the acute and chronic cuprizone ingestion time-courses. Examples of such genes include vimentin (vim), Fgf2, Il1b, nestin (nes), tenasicin c (tnc) and phosphacan (ptprz1). The importance of these genes is that they follow the relative mRNA expression profile of GFAP similarly between time-courses. This means that this particular group of genes might lend themselves to astrocytic manipulation. That is, manipulating the GFAP promoter could influence this group of genes during both the acute and chronic cuprizone ingestion time-courses.

Conversely, the other group of genes highlighted by Figure 9 is the group of genes that has differential correlations to the GFAP relative mRNA profile expression. Examples within this group of genes include transforming growth factor beta receptor (Tgfbr)1, (Tgfbr)2, lymphotoxin beta recptor (Ltbr), Axl and bone morphogenetic factor (Bmp)4. The significance of this group of genes is that they tend to follow the acute relative mRNA expression profile for GFAP more closely than the chronic profile. This means that this particular group of genes exemplifies a pattern of expression different from GFAP at the chronic stages of cuprizone ingestion. Furthermore, this implies that differential OL responses within the cuprizone ingestion paradigm between acute and chronic cuprizone ingestion, is more likely due to this group of genes. One caveat to this statement is that these are only the astroglial-related genes.

There are other genes that have less similar profiles to GFAP and might more responsible for the differential OL response through the cuprizone ingestion paradigm. Nevertheless, the influence of astroglial activation on the differential OL response to demyelination would be most likely due to these genes as opposed to any others.

Other cell type effects on remyelination

Another caveat to the findings of this study is that astrocytes are not the only cell type capable of contributing to the OL response to demyelination. The genes examined in this work for the most part were selected to be representative of factors somehow associated with either astrocytes or oligodendrocytes. The GFAP clustering shows which genes selected are most likely associated with astrocytes and the OL response. However, astrocytes populate demyelinated cuprizone lesions around three weeks of cuprizone ingestion (Matsushima and Morell, 2001). Microglia/macrophages populate the same cuprizone lesion area about the same time, possibly a little earlier (Matsushima and Morell, 2001). While the number of astrocytes within the lesion area tends to stay elevated with more chronic cuprizone feeding, the number of microglia/macrophages tends to decrease with longer time-periods of cuprizone ingestion (Xie et al., 2010). The implication of this observation is that some of astrocyte-related gene regulation observed could actually be a product of activated microglia/macrophages. Particularly, the genes that show a differential Pearson correlation with the GFAP cluster (Figure 9) are the best candidates for microglia/macrophage regulation as opposed to astroglial regulation. This is because those genes with the most similar Pearson correlation to GFAP by

definition follow the relative mRNA expression profile of GFAP. The genes with a different Pearson correlation to GFAP are likely influenced by factors other than just astrocytes.

Chapter V: Development and testing a targeted non-invasive assay for mouse demyelination that can be used in longitudinal studies to assess repair

Introduction/Rationale

The goal of the work presented pertaining to aim three, the development and testing of a non-invasive behavioral assay to detect mouse demyelination status is fourfold. The first goal is to determine the applicability of behavioral testing in longitudinal studies, especially as relevant to recovery of function and remyelination. That is, to establish whether targeted behavioral testing is suited for long-term analyses of the same mice throughout the course of demyelination and subsequent recovery. The second goal is to determine the sensitivity of the behavioral testing for use among small cohorts, as is feasible for remyelination studies. That is, is the behavioral paradigm tested robust enough to detect changes in demyelination status even with small numbers of mice. The third goal is to determine the ability to detect continued effects during chronic demyelination. That is, to ascertain whether the behavioral paradigm can detect deficits associated with demyelination status even after prolonged injury. The fourth goal is to assess motor and non-motor modalities, preferably without interference between measures to allow evaluation using both assays in a given mouse. That is, to establish a complementary behavioral paradigm in which demyelination status corresponds to two independent behavioral measures that can be used in conjunction when establishing the demyelination status of a particular mouse.

Materials and Methods

Mice

Young adult male C57Bl/6 mice were provided from Jackson Laboratories (Bar Harbor ME) at 6 weeks of age and housed singly on-site in the animal facility according to the guidelines of the National Institutes of Health and the Institutional Animal Care and Use Committee of USUHS. All mice were kept on a 12 hour light/dark cycle (0600-1800 light; 1800-0600 dark) in cages that measure 23.62 x 35.3 x 19.56 cm.

Cuprizone Timeline

To induce demyelination mice were fed cuprizone as detailed previously (Chapter II, cuprizone experimental demyelination). For analysis of acute demyelination mice were sacrificed after 6 weeks of continuous cuprizone ingestion. For analysis of chronic demyelination mice were sacrificed after 12 weeks of continuous cuprizone ingestion. For analysis of recovery from acute demyelination, mice were sacrificed after 6 weeks continuous cuprizone ingestion followed by a subsequent 6 week recovery period on normal chow.

Behavioral Timeline

Mouse cohorts were followed longitudinally to compare behavioral performance within subjects in addition to the comparison between subjects. No overt neurological deficits were apparent in treated or non-treated mice. Mice were weighed at the beginning of each week of analysis (0, 6, and 12 weeks of treatment or matched no treatment controls). For the respective 0, 6, and 12 week cuprizone time points, the weights (in grams ± s.d.) for non-treated mice were

24.40 ± 1.21, 26.95 ± 1.94, and 28.37 ± 1.66 while the respective weights for cuprizone-treated mice were 22.42 ± 1.50, 23.28 ± 1.20, and 24.07 ± 0.96 (0 week, $p>0.05$; 6 week, $p<0.001$; 12 week, $p<0.001$; two way ANOVA).

Bilateral sensorimotor limb coordination: Complex Wheel Running Assay

A running assay using wheels with irregularly spaced rungs has been shown to detect functional differences in mice with surgical transection of the corpus callosum (Schalomon and Wahlsten, 2002) and with cuprizone acute demyelination (Liebetantz and Merkler, 2006). These methods were modified to test the application of this assessment for use in longitudinal studies, especially with small cohorts as is feasible for remyelination studies, for detection of continued effects during chronic demyelination, and for use in conjunction with an assessment of non-motor modalities (social interaction assay – see below). Cohorts of mice were housed in cages equipped with an optical sensor to detect the number of wheel revolutions per time interval (Lafayette Instruments, Lafayette IN). A training wheel with all 38 rungs intact was present in the cages for 2 weeks to normalize running behavior. On the third week, mice were introduced to the "complex" wheel with 22 rungs missing at intervals according to the pattern shown (Figure 10A). After the third week, the running wheel was removed from the cage. This cycle of two weeks on the training wheel and one week on the complex wheel has been referred to as a motor skills sequence (MOSS) (Liebetantz and Merkler, 2006). This 3 week sequence was carried out prior to the start of cuprizone and then repeated for the acute, chronic, and recovery time points (Figure 10B). Age, weight and sex-matched control mice were treated identically, but did not have cuprizone in the chow pellets. Using the Activity Wheel Monitoring Software, wheel revolutions were recorded throughout 10 minute intervals during the light phase, when mice were relatively inactive, and throughout one minute intervals during the more active dark phase.

Data from each 24 hour period were exported to a Microsoft Excel file in which total distance run, maximum velocity among daily runs, number of runs, and maximum run interval (i.e. duration of run) were calculated. A total of 29 mice were tested of which 9 were age matched controls. Of the 20 cuprizone treated mice tested, each was tested prior to the beginning of cuprizone feeding in order to serve as a within subjects control. All mice showed spontaneous running activity so that none were excluded on this basis, in contrast to the study by Liebetantz and Merkler (2006).

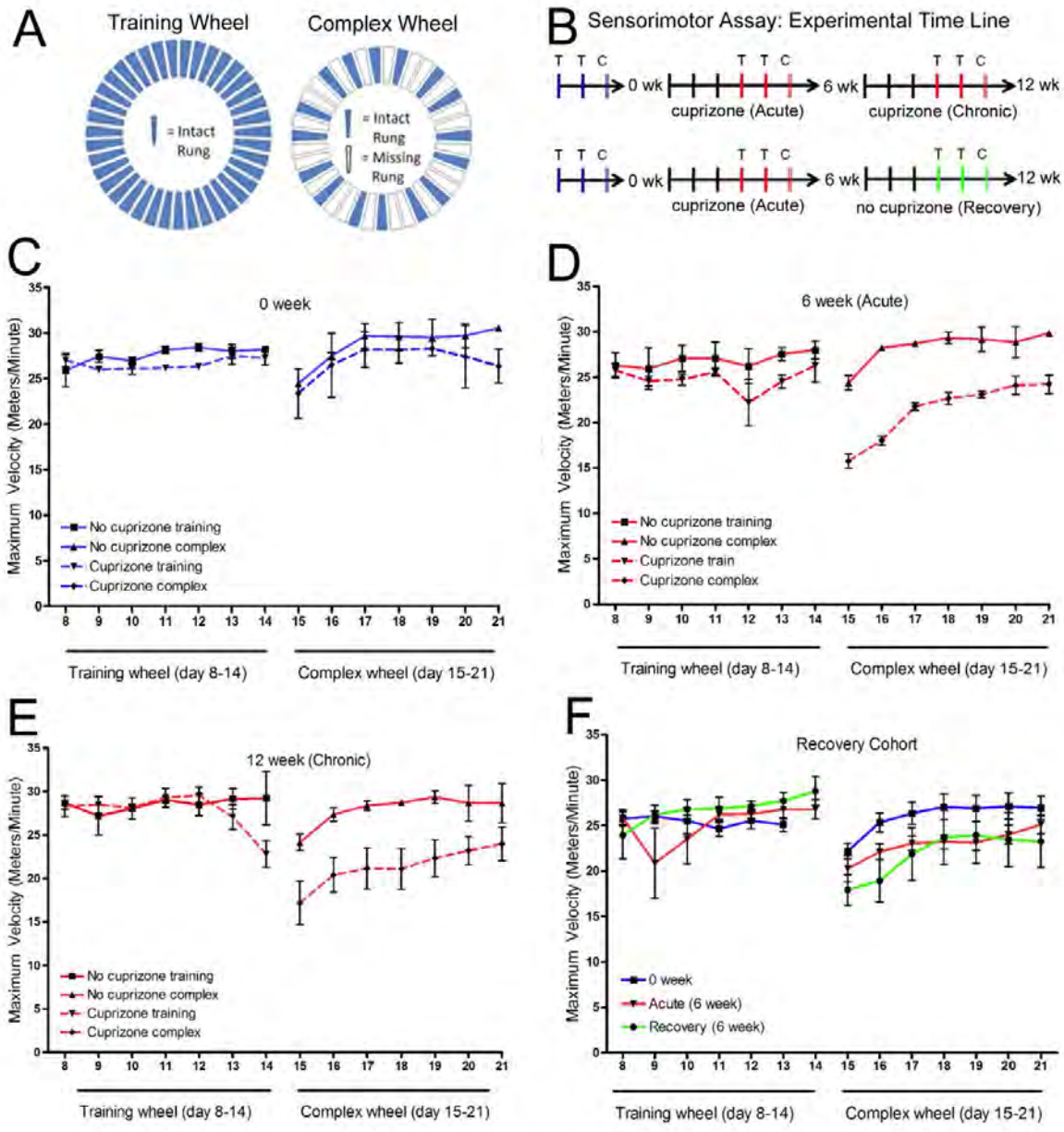
A
Training Wheel
Complex Wheel
= Intact Rung
= Intact Rung
= Missing Rung
B Sensorimotor Assay: Experimental Time Line
T T C
0 wk
6 wk
12 wk
cuprizone (Acute)
cuprizone (Chronic)
no cuprizone (Recovery)
C
0 week
D
6 week (Acute)
E
12 week (Chronic)
F
Recovery Cohort
Maximum Velocity (Meters/Minute)
No cuprizone training
No cuprizone complex
Cuprizone training
Cuprizone complex
Cuprizone train
0 week
Acute (6 week)
Recovery (6 week)
Training wheel (day 8-14)
Complex wheel (day 15-21)

Figure 10. Mice with cuprizone induced demyelination can be distinguished using complex wheel activity that challenges bilateral sensorimotor coordination. A: Home cages were equipped with either a training wheel (all rungs in place) or a complex wheel (one or two rungs removed in an alternating pattern). **B**: Time line showing availability of training wheel (T) or complex wheel (C) in the cages. Each set of wheel availability consisted of one week on the training wheel to stabilize the behavior, a second week on the training wheel to record values, and a subsequent week on the complex wheel. Wheel sets were scheduled so that the complex wheel period ended at the start of cuprizone feeding (0 week, blue), at the end of the acute demyelination phase (6 week, red), at the end of the chronic demyelination phase (12 week, red), or at the end of the 6-week period for recovery following acute demyelination (Recovery, green). **C-F:** The maximum velocity (Vmax) recorded is shown for each 24 hr period. Each graph shows the second week of activity on the training wheel (day 8-14) and the subsequent week on the complex wheel (day 15-21). **C-E:** An example from a matched set of six mice separated into two cohorts of three mice for cuprizone treatment and three non-treated mice. On the training wheel, Vmax values are not significantly different ($p>0.05$) between non-treated mice and those fed cuprizone for any conditions tested. On the complex wheel, Vmax values are not significantly different prior to the start of cuprizone (C; $p>0.05$) but are significantly decreased during week 6 of cuprizone feeding (D; $p<0.0001$) and continue to be significantly lower during week 12 of continuous cuprizone feeding (E; $p<0.0001$). When assessed in parallel with the same mice followed longitudinally, the complex wheel Vmax distinguishes treated from non-treated mice with this small cohort size. **F:** An example of a cohort of six mice followed longitudinally to test the effect of a recovery period that should correlate with significant

remyelination. No significant differences in Vmax were observed on the training wheel within the cohort across disease stages ($p>0.05$). On the complex wheels, compared to the values prior to the start of cuprizone (blue, 0 week), the mice treated with cuprizone for 6 weeks had significantly reduced Vmax values both during week 6 of cuprizone feeding (red vs blue; $p<0.01$) and during week 6 of the recovery period following cuprizone treatment (green vs blue; $p<0.01$). Therefore, during remyelination, the complex wheel Vmax still detected a significant difference among mice that had experienced an episode of demyelination. Figure from (Hibbits et al., 2009).

Social Interaction: Resident-Intruder Assay

As a broad screen of activities, the resident-intruder assay (Bolivar et al., 2007) was modified to use video recording to quantify all distinct behaviors of cuprizone treated and non-treated resident mice in the presence and absence of an intruder mouse in combination with analysis of movement to assess overall activity level and overt neurological differences. Individual cuprizone treated or non-treated C57Bl/6 male mice (with observer blinded to treatment category) were placed in a clean plastic housing cage identical to the home cage (23.62 x 35.3 x 19.56 cm) for 15 minutes to establish each as the "resident" mouse. An age-matched, weight-matched non-treated male mouse was introduced as the "intruder" for a second 15-minute period. Both 15 minute sessions were video recorded to facilitate scoring of all identifiable distinct behaviors. The number of distinct behaviors was scored for the resident mouse (15 minutes alone; 15 minutes with intruder) and for the intruder mouse (15 minutes with resident).

The independent behaviors include sniffing the environment, rearing alongside the cage, rearing independently, digging, circling clockwise, circling counter-clockwise, allogrooming, freezing and scratching. Interactive behaviors include sniffing the other mouse, following, grooming, rearing at the other mouse, sitting or laying next to the other mouse, backing or running away from the other mouse, biting, boxing or wrestling, mounting, pinning and tail-rattling. Video files were also analyzed using an ObjectTracker program on ImageJ (Bethesda, MD). This analysis yielded Microsoft Excel data files with object coordinates within the cage for every one second of video recording. From these data sets the distance traveled for each 15 minute video recording session was extrapolated. Unpaired t-tests were used to assess differences between age-matched cohorts for both independent and interactive behaviors. A total

of 46 resident mice (25 cuprizone treated and 21 non-treated matched controls) were examined using the resident-intruder assay.

Analysis of myelination status

In addition to corpus callosum myelination (described in Chapter II), the quantification of cerebral cortex myelination was estimated from MOG immunofluorescence in the same tissue sections used for CC analysis. Pixel intensity values were normalized between sections by thresholding to distinguish myelinated cortical radiation fibers in the cortex. The percent area of the cortex (over the CC from the midline unilaterally to over the apex of the cingulum) with MOG immunoreactivity above the threshold level was then used as an estimate of the myelinated area.

Statistical analysis

For each experimental approach, each category analyzed included three or more mice per condition. Analysis of tissue sections included at least three sections per mouse. Prism 5.0 (GraphPad Software, San Diego, CA) was used for statistical analyses. Unpaired t-tests were used to assess differences between age-matched cohorts for a single time point. One-way ANOVA with post hoc Tukey's multiple comparison was used to determine significant differences across time points. Two-way ANOVA with post hoc Tukey's multiple comparisons was used for analysis across time points and treatments. Statistical significance was determined as $p < 0.05$.

Results

Complex wheel assay of bilateral sensorimotor coordination

Although the CC is a common site for analysis of demyelination and remyelination for many reasons, including those noted above, these analyses are constrained by the lack of a measure of CC function that can be applied in longitudinal studies to monitor the effect of demyelination as well as to functionally evaluate manipulations to promote remyelination. Cuprizone ingestion results in widespread, reproducible demyelination of the CC in mice (Matsushima and Morell, 2001; Mason et al., 2001; Armstrong et al., 2002, 2006) making the cuprizone model ideal for testing functional behavioral correlates of CC myelination status. A complex wheel assessment that incorporates irregularly spaced wheel rungs was selected for longitudinal analysis of CC function because of the required integration of sensory and motor information bilaterally in a non-uniform pattern, which would reduce the influence of pattern-generating spinal cord locomotion expected to correspond with uniform or rhythmic movements (Figure 910, B). Differences detected with the complex wheel assay have been previously correlated with surgical transection of the CC (Schlamomon and Wahlsten, 2002) and with acute (6 week) cuprizone treatment (Liebetantz and Merkler, 2006).

The parameters recorded daily from the wheel running behavior included the total number of runs, total distance run, maximum run interval, and the maximal running velocity (Vmax). The Vmax appeared to be a relevant parameter for the complex wheel differentiation of bilateral sensorimotor coordination as shown for a representative cohort of mice in Figure 10C-D. Baseline measures of Vmax were recorded on the training wheel and the complex wheel for all mice prior to the start of cuprizone treatment. No differences in baseline values were observed between the cohorts of mice tested (0 weeks; Figure 10C). Compared to the matched non-treated cohort, the treated mice had slower Vmax values on the complex running wheel after both acute (6 weeks; $p<0.0001$) and chronic (12 weeks; $p<0.0001$) cuprizone ingestion (Figure 10D, E).

During the week on the complex wheel the sum of the Vmax values was reduced 24.7% for mice fed cuprizone for 6 weeks and 23.7% for mice fed cuprizone for 12 weeks, with each compared to the respective matched cohort. These results indicate that the Vmax values exhibit significant differences during both acute and chronic stages that are not abrogated from the repeated exposure to the complex wheel in these longitudinal studies. Values for the other wheel running parameters had greater variability than Vmax and during chronic demyelination did not distinguish treated from non-treated mice on the complex wheels (number of runs, $p = 0.8369$; maximum run interval, $p > 0.05$), with the exception of the total distance run ($p < 0.01$) which had velocity as a contributing factor. Also, on the training wheels, Vmax values were not significantly different between the cuprizone treated and non-treated mice throughout the time course (Figure 10C-E). Therefore, the complex wheel can detect motor coordination deficits that are not apparent with the uniformly spaced rungs on the training wheel. This lack of differences on the training wheel also indicates that the cuprizone treatment did not cause an overall decrease of interest in the wheel or impair the general ability to run rapidly.

Mice were also tested longitudinally at time points of before cuprizone (0 week), after acute demyelination (6 weeks of cuprizone) and again after a period for recovery (6 weeks on normal chow) (Figure 10F). Again, Vmax values on the training wheel were not significantly different among mice tested at different disease time points. In contrast, the mice had significantly slower Vmax values on the complex wheel at the acute (reduced 11.5%) and recovery (reduced 15.8%) time points than at the pre-cuprizone time point (Figure 9F; $p<0.01$ for each time point). The values did not change significantly between the acute and recovery time points on the complex wheel (Figure 10F). These findings indicate that Vmax on the complex wheel is sensitive to demyelination status both between and within-subjects. Furthermore, the complex wheel Vmax

values indicated continued effects on this behavior even after a 6-week period for recovery that is typically associated with extensive remyelination, indicating continued neurophysiological abnormalities.

Resident-intruder paradigm for assessment of social interaction

A social interaction paradigm was tested as a distinct behavioral assessment to complement the sensorimotor assessment from the complex wheel assay. The resident-intruder test of social interaction (Bolivar et al., 2007) was modified to evaluate overt neurological function and to quantify overall activity as well as all distinct behaviors identified for each mouse (Figure 11A). The resident mouse was either cuprizone-treated or a non-treated control while the intruder mouse was always a non-treated control. No overt neurological symptoms were observed in any of the mice examined during acute or chronic cuprizone treatment. Overall distance traveled during the recording period was calculated to determine whether a difference in overall movement of the mice may contribute to the increased interactive behaviors observed (Figure 11B). This analysis of movement showed no difference in total distance traveled between cuprizone treated animals and age-matched controls. Across the battery of activities recorded, a grouping became apparent in that interactive behaviors were consistently increased in frequency among mice with acute demyelination (6 weeks cuprizone) compared to the control cohort. Conversely, independent behaviors were consistently less frequent among the mice with acute demyelination.

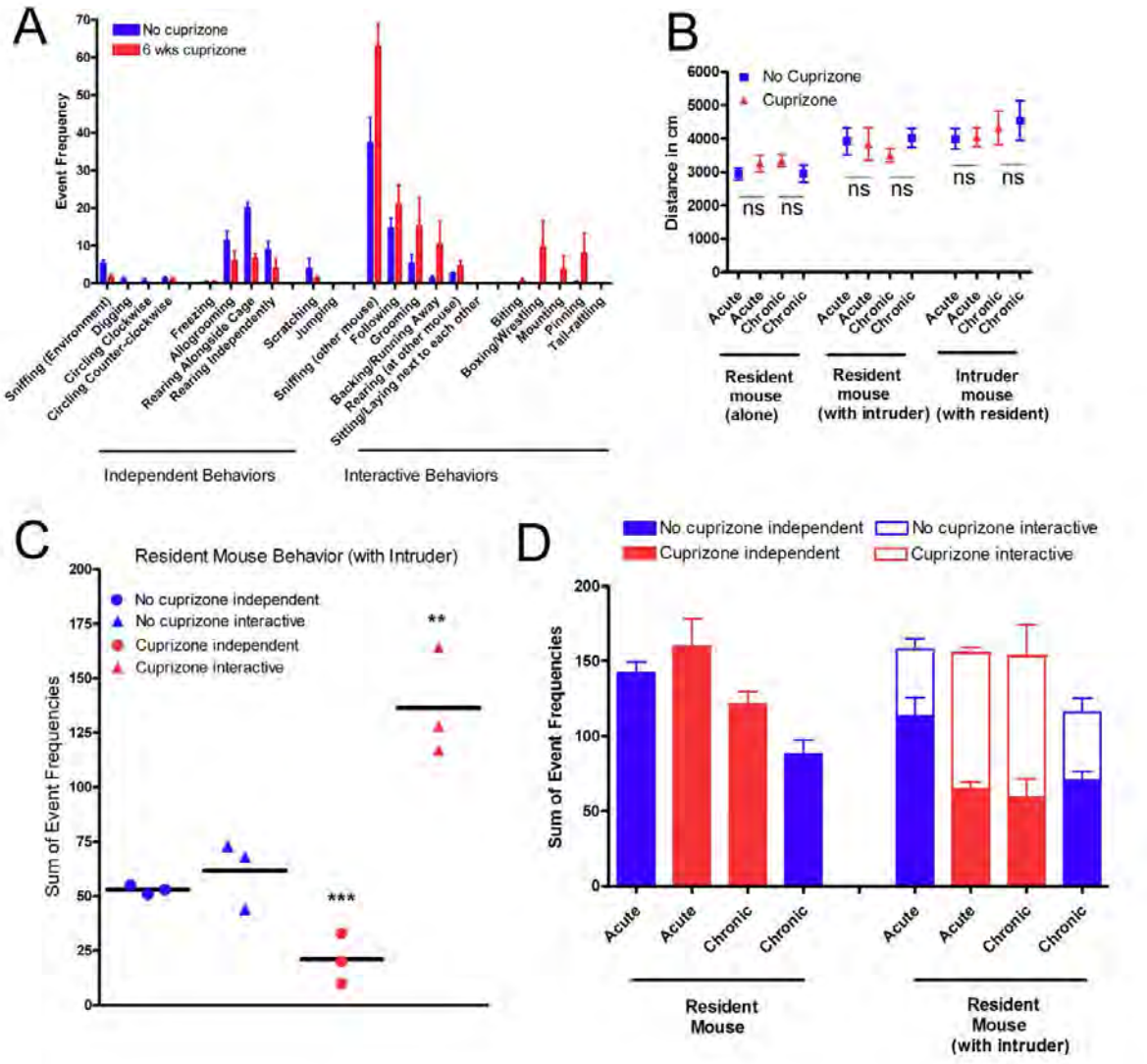
A
No cuprizone
6 wks cuprizone
Event Frequency
Sniffing (Environment)
Digging
Circling Clockwise
Circling Counter-clockwise
Freezing
Allogrooming
Rearing Alongside Cage
Rearing Independently
Scratching
Jumping
Sniffing (other mouse)
Following
Grooming
Backing/Running Away
Rearing (at other mouse)
Sitting/Laying next to each other
Biting
Boxing/Wrestling
Mounting
Pinning
Tail-rattling
Independent Behaviors
Interactive Behaviors
B
No Cuprizone
Cuprizone
Distance in cm
ns
Acute
Chronic
Resident mouse (alone)
Resident mouse (with intruder)
Intruder mouse (with resident)
C
Resident Mouse Behavior (with Intruder)
No cuprizone independent
No cuprizone interactive
Cuprizone independent
Cuprizone interactive
Sum of Event Frequencies
**
***
D
No cuprizone independent
No cuprizone interactive
Cuprizone independent
Cuprizone interactive
Sum of Event Frequencies
Resident Mouse
Resident Mouse (with intruder)

Figure 11. Mice with cuprizone induced demyelination can be distinguished using the resident-intruder social interaction paradigm. **A**: An example of the battery of distinct behaviors quantified among mice filmed during the period with both a resident mouse (with or without cuprizone feeding) and an intruder mouse (always without cuprizone) in the cage. Grouping of behaviors according to treatment condition reveals that, compared to non-treated mice (blue), mice treated with cuprizone for 6 weeks (red) have a lower frequency of behaviors that can be categorized as "independent" and a higher frequency of behaviors involving the intruder mouse that can be categorized as "interactive" behaviors (n = 3 for each cohort of mice). **B**: Total distance traveled during each filming was measured as an indicator of overall activity. In each condition, no significant differences were observed in acute (6 week) or chronic (12 week) cuprizone treated mice relative to the age-matched control mice (n = 3 for each cohort of mice; all comparisons, $p>0.1$). **C:** Resident mouse behavior frequencies were combined to sum those that indicated independent or interactive events, as noted in panel A. The cuprizone treated mice showed significantly decreased independent behaviors and more dramatically elevated interactive events (n = 3 mice per condition; $p = 0.0091$ and $p = 0.0112$, respectively). Values for individual resident cuprizone treated mice separated clearly from control mice. **D:** Comparison of cohorts of acute and chronic cuprizone treated mice with age-matched controls. In the absence of an intruder mouse, an age-dependent decrease of independent activities is observed across this prolonged disease time course ($p = 0.0007$). There is a marginally significant treatment effect among the resident mice while observed alone ($p = 0.0436$). In the presence of an intruder mouse, resident mice treated with cuprizone had a significantly decreased frequency of independent behaviors ($p = 0.0045$) and increased

frequency of interactive behaviors ($p = 0.0028$) compared to the age-matched non-treated mice. In the presence of an intruder mouse, there was again an age-dependent effect among the independent behaviors ($p = 0.018$). Statistical comparisons are from two-way ANOVA with 6 mice per group. Figure from (Hibbits et al., 2009).

The social interaction data was further analyzed to determine whether significant differences could be demonstrated for individual mice within each cohort (Figure 11C). To take advantage of the distribution of behaviors observed (Figure 11A) the set of activities quantified was summed for independent versus interactive behaviors. Individual mouse values clearly separate based on treatment condition. Indeed, the interactive behaviors for each acute cuprizone treated mouse are clearly distinct from the values for the non-treated mice.

This distinction of interactive versus independent behaviors was also tested for applicability across acute through chronic demyelination stages (Figure 11D). Compared to the matched controls, the resident mice with acute demyelination showed a significant shift of behaviors with a 51.0% increase in interactive behaviors and 42.9% decrease in independent behaviors. Importantly, the mice with chronic demyelination continued to show an increase of interactive behaviors (49.2%). These differences in treated versus non-treated mice across both time points were significant based on a two-way ANOVA analysis (interactive behaviors, $p = 0.0028$; independent behaviors, $p = 0.0045$). It should also be noted that among the separate cohorts of mice that a decrease of independent activity frequency was observed, which was most notable between ages among the control mice, indicating an age-dependent effect among the resident mice ($p = 0.0007$ without intruder; $p = 0.018$ with intruder). Therefore, the frequency of interactive behaviors appears to be a better parameter than independent behaviors for comparisons across this prolonged disease course.

Resident mice with acute demyelination followed by a 6-week recovery period still showed a high frequency of interactive behaviors (111.7 ± 18.9) and low frequency of independent behaviors (61.3 ± 18.6) in the presence of the intruder mouse. Although only a set of three mice

was tested for this recovery cohort, the values are very close to those of the acute and chronic cohorts, indicating a lack of functional recovery during the remyelination period that is also consistent with the lack of full recovery on the complex wheel (Figure 10F). Ideally, direct comparison of values for the same mice evaluated at both the acute and recovery time points would be optimal to evaluate changes longitudinally, which was not done with this recovery cohort. In general, mice should be socially naïve before testing in a resident-intruder paradigm (Bolivar et al., 2007). Therefore, this social interaction paradigm is not expected to be appropriate for repeated testing of the same resident mouse for longitudinal studies, presumably because repetition may dampen interest of the resident mouse to interact with the novel intruder mouse. Surprisingly, we performed a preliminary test of a matched cohort of treated (n = 3) and non-treated (n = 3) mice evaluated at both 6 and 12 weeks of cuprizone and found significant differences across both acute and chronic stages ($p = 0.0427$ for independent behaviors, $p = 0.0186$ for interactive behaviors; two-way ANOVA). This finding may reflect that the cuprizone effect is unusually robust for this behavioral assay and so maintained a significant difference upon repetition. However, the major advantage of the resident-intruder social interaction paradigm is for analysis on a specific day during the course of demyelination in that the video recording can be accomplished in an hour and requires no specific training of the mice.

Myelination status of mice used in behavioral studies

Upon completion of behavioral assessments, coronal sections through the body of the CC were immunostained for MOG to estimate the myelination status at specific stages of cuprizone treatment and recovery (Figure 12). The expected demyelination of the CC after 6 and 12 weeks of continuous cuprizone ingestion is evident when compared to normally myelinated non-treated control mice (Figure 12A, C-E; $p = 0.0027$ for both 6 and 12 weeks of cuprizone compared to

control values). In addition, after acute demyelination, extensive spontaneous remyelination of the CC is evident following the subsequent 6 weeks of recovery on normal chow (Figure 12A, F). Myelination of the adjacent cerebral cortex was also examined for a potential contribution to the observed behavioral effects. There was significant demyelination in the cerebral cortex after chronic cuprizone treatment ($p = 0.0207$) but not following acute cuprizone treatment (Figure 12B, C-E).

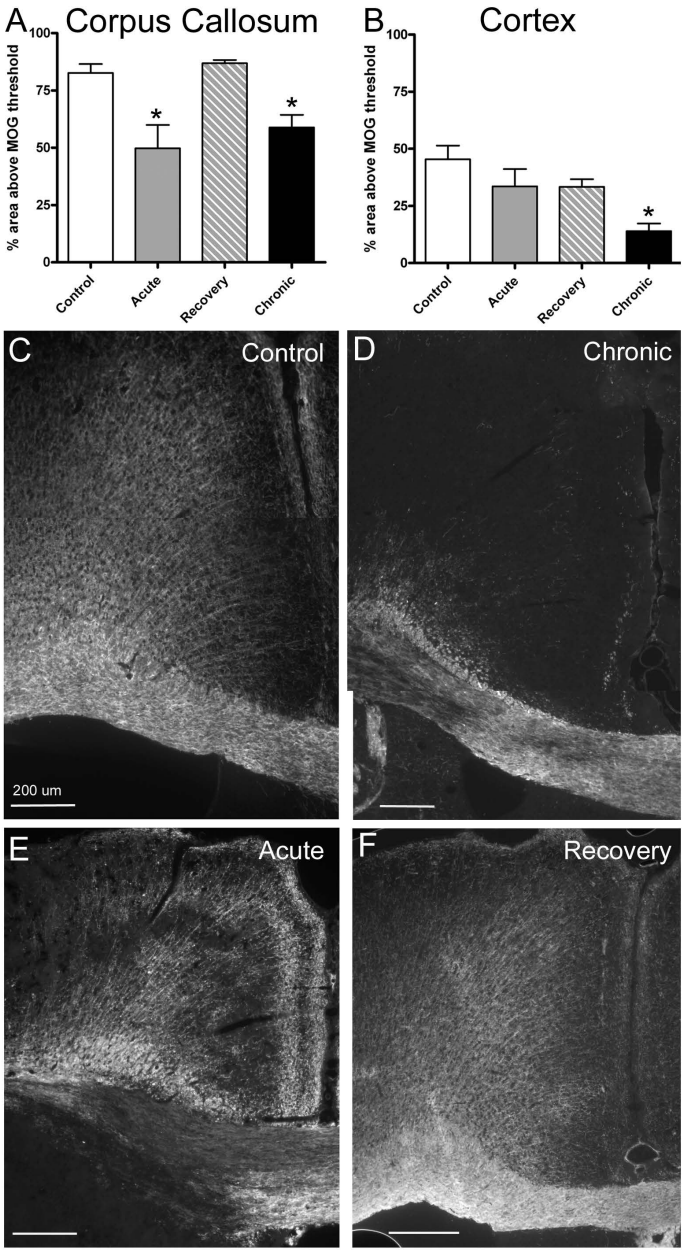
A
Corpus Callosum
% area above MOG threshold
100
75
50
25
0
*
*
Control
Acute
Recovery
Chronic
B
Cortex
% area above MOG threshold
100
75
50
25
0
*
Control
Acute
Recovery
Chronic
C
Control
200 um
D
Chronic
E
Acute
F
Recovery

Figure 12. Quantitative analysis of myelination following behavioral assessments. A, B: Corpus callosum (A) and cerebral cortical (B) myelination was estimated in coronal brain sections based on the percent area immunolabeled for myelin oligodendrocyte glycoprotein (MOG). The region analyzed for the corpus callosum (CC) extended from the midline to under the apex of the cingulum. The region analyzed in the adjacent cerebral cortex was outlined from the midline along the pial surface with the lateral border parallel to the midline down to the apex of the cingulum and continuing with the inferior boundary as the border with the cingulum and CC. **A:** Compared to non-treated control mice, during cuprizone treatment myelination of the CC was significantly reduced at acute (6 weeks; $p = 0.0027$) and chronic (12 weeks; $p = 0.0027$) time points while the percent area myelinated returned to control levels in the mice allowed a recovery period (6 weeks of cuprizone feeding followed by 6 weeks on normal chow). **B:** Compared to non-treated mice, only the chronic (12 week) cuprizone condition showed a significant reduction of the percent area myelinated in the adjacent cortical region ($p = 0.0207$). **C-D:** Representative images of immunofluorescence for MOG to illustrate myelination patterns in the CC and adjacent cortex in coronal sections. Comparison with a non-treated mouse (C, Control) shows demyelinated areas in both the CC and adjacent cortex after 12 weeks of cuprizone treatment (D, Chronic). After cuprizone treatment for 6 weeks (E, Acute) demyelination is much more apparent in the CC than in the adjacent cortex and the CC is no longer markedly demyelinated after a subsequent 6 week period on normal chow (F, Recovery). Scale bars = 200 μm. Figure from (Hibbits et al., 2009).

To evaluate myelination status in additional neuroanatomical areas for which cuprizone demyelination has been reported, we also performed MOG immunohistochemistry on coronal

brain sections at more caudal levels to include hippocampal areas and on sagittal sections through the cerebellum (Figure 13). Demyelination of hippocampal fibers was evident after 6 weeks of cuprizone in the dorsal hippocampal commissure and within the hippocampus, which was especially marked in the hilus area in comparison with non-treated mice (Figure 13A, B). In contrast, the cerebellar tissue did not show evidence of demyelination in the arbor vitae or the cerebellar cortex even when examined after 12 weeks of cuprizone treatment (Figure 12C). Therefore, the behavioral changes observed correlate with demyelination of the CC with co-incident demyelination in hippocampal fibers.

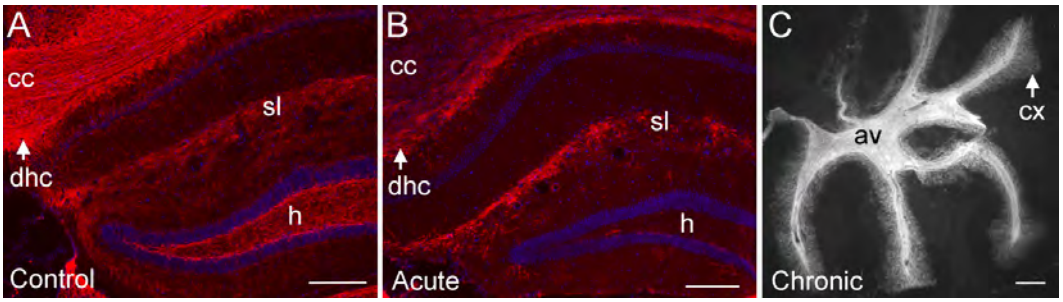

Figure 13. Myelination of hippocampal and cerebellar regions. A, B: MOG immunohistochemistry in coronal brain sections shows myelinated hippocampal fibers in non-treated mice (A) that are markedly reduced in mice with acute demyelination following 6 weeks of cuprizone treatment (B). cc = corpus callosum, dhc = dorsal hippocampal commissure, h = hilus, sl = stratum lacunosum of CA1. **C:** MOG immunohistochemistry in a sagittal section through the cerebellum shows heavy myelination of the arbor vitae (av) with myelinated fibers extending throughout the cerebellar cortex (cx), which illustrates a lack of cerebellar demyelination in mice treated with cuprizone for 12 weeks. Scale bars = 200 µm. Figure from (Hibbits et al., 2009).

Chapter VI: Discussion of results and implications

Summary of research findings in this work

In this work research is presented pertaining to the limited remyelination that occurs after chronic or prolonged demyelination. The three specific aims addressed in this work concentrated on identifying and characterizing possible cellular mechanisms contributing to remyelination potential and also on developing a method for non-invasively assessing demyelination status in mice. Apoptosis was identified as an *in vivo* a contributor to limited remyelination after chronic cuprizone ingestion. Astrogliosis was characterized as occurring to the extent of severe diffuse reactive gliosis without compact glial scar formation after both acute and chronic demyelination. Non-invasive targeted behavioral assays were described revealing functional impairment related to CC cuprizone induced demyelination in mice. These assays can be used to behaviorally phenotype mice based on demyelination status.

Implications of this work for demyelinating disorders particularly MS

The ultimate goal of all the studies presented in this work is to promote remyelination after episodes of chronic or prolonged demyelination in an effort not only attain functional recovery, but also as means to prevent permanent long-term disability. MS is the leading cause of demyelination worldwide. It often has a long disease progression and is characterized by demyelination throughout the disease course. Functional impairments attributed to demyelination arise from impaired axonal conduction, which is a direct consequence of demyelination.

Furthermore, demyelination leaves axons denuded, making them more vulnerable to damage and loss compared to fully myelinated axons. In MS long-term functional impairments are the result of such axonal loss (Lassmann, 2011). Remyelination therefore, is not only a method to restore conduction in viable axons, but is also a method of neuroprotection.

Use of rodent models of demyelination

The interplay of many different cell types and signaling mechanisms contribute to remyelination potential. Though the context of demyelination is most relevant to human patients with MS, specific and controlled analysis of the mechanisms contributing to remyelination potential are best studied using animal models. Acute demyelination models often show robust spontaneous remyelination (Kipp et al., 2009; Hanafy and Sloane, 2011; Kotter et al., 2012), but do not accurately mimic the disease state with more chronic and prolonged demyelination episodes and a limited OL progenitor pool (Armstrong et al., 2002; Chang et al., 2002; Mason et al., 2004; Back et al., 2005; Armstrong et al., 2006).

Detection of cuprizone-induced demyelination in the CC

Demyelination of the CC caused by cuprizone ingestion can be observed with histopathological and immunohistochemical stains. In each of the studies described in this work, demyelination is assessed with MOG immunoreactivity in the CC, which gives an indication of the percent myelinated area. Though myelination status can be detected with a variety of different staining protocols, the extent to which changes in myelination are evident at specific stages following cuprizone treatment might vary with the detection methodology. Electron microscopic quantification of myelination in the CC (Lindner et al., 2008) correlates

with LFB staining and MOG immunoreactivity to a greater degree than with immunoreactivity for PLP or and MBP. Moreover, the MOG immunoreactivity presented in these studies are consistent with previous data from our lab showing demyelination in response to cuprizone (Armstrong et al, 2006, Figure 2, Figure 10). In addition, LFB myelin staining (Armstrong et al., 2002; Song et al., 2005) correlates well with this MOG immunoreactivity (Armstrong et al., 2006; Figure 2, 10) and with findings reported by other labs using cuprizone (e.g. Matsushima and Morell, 2001). The implication of these observations is that the MOG immunohistochemistry data presented are good indicators of myelination status. Furthermore, the cuprizone model used in this work produced demyelination as expected (Armstrong et al., 2006; Vana et al., 2007; Xie et al., 2010), in the mice analyzed, indicating that the observations made are at least partially attributable to demyelination status.

Correlation between cuprizone demyelination and MS pathology

In contrast to acute demyelination models, the cuprizone ingestion paradigm in mice is a particularly good model for the study of chronic demyelination with limited remyelination. Cuprizone administration can be regulated over a specific time-course to assess the temporal effects of demyelination. Furthermore, chronic cuprizone ingestion produces a limited remyelination capacity as the amount of spontaneous recovery decreases after chronic cuprizone ingestion is ceased. Moreover, the OL progenitor pool is depleted as a consequence of chronic cuprizone ingestion (Armstrong et al., 2002; Mason et al., 2004; Armstrong et al., 2006), which reflects the MS disease where the OL progenitor pool is also depleted (Mason et al., 2001; Mason et al., 2004; Woodruff et al., 2004).

In this work, the cuprizone ingestion paradigm was used to induce different time-courses of demyelination and remyelination. Cuprizone ingestion is known to induce a reproducible pattern of extensive CC demyelination in mice (Matsushima and Morell, 2001; Mason et al., 2001; Armstrong et al., 2002, 2006). The CC is a well suited model for the study of demyelination and remyelination as it has a close proximity to the SVZ and SVG, which are germinal zones that show elevation of proliferation in response to cuprizone (Gallo and Armstrong, 2008), indicating a good repair potential.

Astrogliosis in cuprizone-induced demyelination corresponds with astrogliosis in MS lesions

Furthermore, severe diffuse reactive astrogliosis without compact glial scar formation, as occurs in cuprizone induced demyelination is characteristic of some MS lesions (Lucchinetti et al., 2000; van der Valk and De Groot, 2000; Lassmann, 2011), demonstrating not only the association of the cuprizone model with the human disease state, but also suggesting the potential for remyelination in such lesions (Chang et al., 2002; Holley et al., 2003; Kotter et al., 2011). For example, only active demyelinating MS lesions express high levels of fibronectin, compared to inactive MS lesions and normal white matter with little fibronectin expression (Sobel and Mitchell, 1989). Along these lines, proliferating astrocytes are more characteristic of early active and early remyelinating MS lesions as compared to normal white matter, late active, demyelinated or late remyelinating MS lesions (Schonrock et al., 1998).

Interestingly, apoptosis is also characteristic of early active MS lesions as opposed to more chronic MS lesions (Breij et al., 2008). Taken together, these observations indicate that the level of demyelination observed in the cuprizone ingestion paradigm corresponds most closely with

early MS lesion activity. It is possible that early remyelination activity is also indicated. At the very least, the stage of demyelination in the cuprizone model does not actively hinder remyelination with the formation of a compact glial scar even in the chronic cuprizone ingestion time-course.

Implications of continued astroglial activation during demyelination

While astroglial activity can be characterized as occurring to the same extent in both the acute and chronic cuprizone ingestion time-courses, definitively attributing the astrocytic-related gene constellation to this particular stage of severe diffuse reactive astrogliosis without compact glial scar formation is more difficult. Decreases in relative mRNA expression of astrocyte-related gene transcripts during the time-course of cuprizone ingestion (Table 1, 2) indicate that astrogliosis does not cease after initial cuprizone administration. Rather, astroglial-related genes increase in relative fold mRNA expression levels during the entire course of cuprizone ingestion (Figure 8), in both the acute (Table 1) and chronic (Table 2) cuprizone ingestion and recovery time-lines. It is only after return to normal chow that astroglial-related genes begin to return to control levels (Figure 8, Table 1, 2). This indicates that continued astroglial activation might play a role in determining the stage of astroglial activation observed in the cuprizone model.

Assessing functional remyelination potential in the human CC

Assessing the functional effectiveness of such manipulations is a challenging prospect. As mentioned, the CC is well-suited and widely used for studies of demyelination and remyelination (Armstrong et al., 2002; Mason et al., 2004; Armstrong et al., 2006; Vana et al.,

2007; Lindner et al., 2008; Groebe et al., 2009). Impairments of the CC in humans are associated with impairments in complex interhemispheric functions. Some of these impairments are related to language skills (Friederici et al., 2007), dichotic listening (Gadea et al, 2009), bimanual finger opposition movements (Bonzano et al., 2008) and social interaction and social communication (Badaruddin et al., 2007) have been reported. In addition, abnormal CC development has also shown correlations in autism spectrum disorders (Cody et al., 2002; Nicolson and Szatmari, 2003; Alexander et al., 2007; Anstey et al., 2007; Paul et al., 2007).

Assessing functional remyelination potential in the rodent CC

Despite human studies suggesting behavioral outcomes for CC impairment, modeling such outcomes in experimental animals is difficult. Moreover, studies pertaining to the functional behavioral outcomes of CC demyelination in mice, the prototypical animal model used for CC demyelination studies, are limited. The few studies examining CC function in rodents have established consistent findings for social interactions and bilateral coordination. Sociability measures have been correlated with CC size among mouse strains (Fairless et al., 2008) and bilateral limb coordination, as assessed by wheel running on a complex wheel, exhibited deficits as a result of CC agenesis or callosotomy (Schalomon and Wahlsten, 2002) and acute cuprizone demyelination (Liebetanz and Merkler, 2006).

In an attempt to establish a non-invasive targeted behavioral assay for the analysis of mouse demyelination status, both bilateral sensorimotor coordination and social interaction assessments for complementary tests of CC function for studies of cuprizone induced demyelination in mice were employed. The results indicate that both a complex wheel test of

sensorimotor coordination and a resident-intruder test of social interaction correlate with CC demyelination status to test distinct functional modalities independently or in conjunction with one another. The complex wheel assay maintains sensitivity when performed at repeated intervals for longitudinal analyses. Both assays distinguish treated from control mice during both acute and chronic demyelination. In addition, both assays are extremely sensitive and detect significant differences between cohorts as small as three mice. Additionally, the data distinguish treated from non-treated mice following acute demyelination and subsequent recovery period with spontaneous remyelination, indicating that normal action potential transmission has not yet fully recovered along previously demyelinated axons. These behavioral measures of CC function in mice are important to non-invasively monitor demyelination as well as to functionally evaluate manipulations to promote remyelination.

Motor deficits correspond with CC demyelination in mice

Consistent with predicted coordination deficits with CC demyelination, several recent reports indicate motor activity deficits with cuprizone treatment in C57bl/6 mice but do not demonstrate applicability for longitudinal studies. After 5 weeks of cuprizone ingestion, deficits are evident as an increase in the frequency of falls on the rotarod although the sensitivity of the rotarod to measure CC myelination status is unclear since a significant difference was not found at 6 weeks of cuprizone but was present after 6 weeks of cuprizone and 6 weeks of recovery (Franco-Pons et al., 2007). Wheel running with a sequence of training and complex rung patterns showed significant differences in maximal velocity on the complex wheel at 6 weeks of cuprizone treatment (Liebetanz and Merkler, 2006), as was confirmed in the current studies

(Figure 1). Both the rotarod and complex wheel assays indicate that significant differences continue even after a 6-week recovery period for remyelination (Liebetanz and Merkler, 2006; Franco-Pons et al., 2007).

Importance of longitudinal assessments for mouse CC function

Each of these previous studies tested activity only at one time point prior to sacrifice so that comparison could only be made between separate cohorts sacrificed at each disease stage. Importantly, the current study was designed to determine whether the complex wheel assessment would be sufficiently sensitive when repeated on a given mouse, as needed for longitudinal studies, or when used to analyze small cohorts of mice, as would be practical in typical remyelination studies. Factors such as training and novelty effects can influence the use of behavioral assessments for repeated measures in longitudinal studies. As our results demonstrate, the complex wheel assay can be used for a within-subjects comparison of pre-treatment, demyelination, and remyelination time points. In addition, significant differences were observed with cohorts of only three mice in the current study design as compared to typically larger cohort sizes in behavioral studies, such as the design in the acute cuprizone study with a complex wheel assessment that used 12 mice per cohort (Liebetantz and Merkler, 2006).

Other behavioral measures for mouse CC function

Behavioral assessments of anxiety, memory, and social interaction have also been reported with cuprizone treatment in C57Bl/6 mice (Franco-Pons, et al. 2007; Xu et al. 2009). In contrast to our findings of increased interactive behaviors among the cuprizone treated mice in the resident-intruder assay (Figure 2), Xu et al. (2009) reported significantly decreased social interaction among mice treated with cuprizone for 4-6 weeks. However, the analysis of social

interaction used by Xu and colleagues was automated and based on the two mice being closer than 5 cm for 0.2s without being validated by manual observation of an interactive behavior involving both mice as was quantified in the current study. Furthermore, open field assessments in cuprizone treated mice showed a tendency toward the field center (Franco-Pons et al., 2007; Xu et al., 2009), indicating decreased anxiety which may be consistent with the increased interactive behaviors observed in our resident-intruder assays. Spatial working memory deficits were similar at weeks 2, 3, 4, 5, and 6 of cuprizone treatment (Xu et al., 2009), indicating a poor correlation of these assessments with the dramatic changes of myelination status of the CC over this time course.

Relevance of the social interaction resident-intruder assay for assessing mouse CC function

In this work, using the resident-intruder assay, the increase of interactive behaviors was evident at both acute (6 week) and chronic (12 week) cuprizone treatment stages, which correlates well with significant CC demyelination at each time point. We also noted an age-dependent effect on the frequency of independent behaviors in the resident-intruder assay over this prolonged disease time course. This age effect was not as evident among cuprizone treated resident mice when an intruder was present but may be masked in the treated mice since the level of independent behaviors is already reduced significantly by the treatment effect in the younger mice. To minimize the potential involvement of this age effect among independent behaviors, the frequency of interactive behaviors is likely to give a more direct differentiation of treated versus non-treated mice.

Correlation of behavioral analyses with CC demyelination status

At the completion of the behavioral analysis, the progression of demyelination and remyelination was quantified using immunohistochemistry for MOG, which correlates well with ultrastructural measures of remyelination (Lindner et al., 2008). The findings of deficits in the complex wheel running and of increased interactive behaviors were consistently observed during both acute and chronic demyelination (Figures 9 and 10). Both time points correlate with the presence of extensive demyelination in the corpus callosum (Figure 11). The proportion of CC demyelination at 12 weeks of cuprizone treatment in our mice exposed to the running wheels is similar to that observed at this time point in a previous analysis (Armstrong et al., 2006). Following acute demyelination, spontaneous remyelination of the CC was observed which was also consistent with previous studies (Armstrong et al., 2006). Therefore the wheel access, which is a form of behavioral enrichment, is unlikely to have altered the extent of CC demyelination or remyelination obtained relative to the standard cuprizone protocol. Interestingly, evidence of remyelination during the recovery period after acute demyelination was not accompanied by a similar return of normal activity, indicating that the complex wheel assay is sensitive to persisting abnormalities, possibly in the nodal or other axon-myelin structures.

Targeting mouse CC demyelination with behavioral analyses

Also, cuprizone demyelination, though reproducibly evident in the CC, likely affects other brain areas as well. The CC, as the largest myelinated white matter tract in the brain, along with its reliable susceptibility to cuprizone intoxication, is the area most frequently examined for studies of demyelination and remyelination. Indeed, studies evaluating specific *in vivo* cellular mechanisms underlying demyelination and remyelination are well suited for analysis with cuprizone ingestion. Such studies use the CC as reliable marker of demyelination status within

the organism but generally do not attempt to correlate that status with functional behavioral outcomes. For this reason, specific analysis of CC demyelination status is sufficient for addressing the first two aims of this work.

In contrast, addressing the third aim of this work, which involves developing a targeted non-invasive behavioral assay for demyelination status in mice, requires demyelination analysis of brain regions potentially involved in the manifestation of observed behaviors and also potentially affected by cuprizone administration. Recent reports indicate cuprizone induced demyelination of the cerebral cortex (Gudi et al., 2009) as well as the hippocampus (Norkute et al., 2009) and cerebellum (Groebe et al., 2009). However, after 6 weeks of cuprizone treatment, significant cortical demyelination was not detected with LFB staining (Skripuletz et al., 2008) but was readily detected by immunoreactivity for PLP and MBP (Skripuletz et al., 2008; Gudi et al., 2009). Hippocampal and cerebellar cortical demyelination has also been reported in the murine cuprizone model (Koutsoudaki et al., 2009; Norkute et al., 2009; Skripuletz et al., 2009). As with the cerebral cortex, hippocampal demyelination was noted with PLP immunostaining but was not detected with LFB staining through 6 weeks after cuprizone treatment (Koutsoudaki et al., 2009). While demyelination of hippocampal fibers, including the dorsal hippocampal commissure at 6 weeks after cuprizone treatment has been observed in this and previous studies, with both LFB staining and with MOG immunohistochemistry (Armstrong et al., 2002, Song et al., 2005; Figures 10) the same studies indicate that cerebral cortical demyelination is not marked at this time-point (Figure 11). In addition, cerebellar cortical demyelination was not apparent in preliminary analysis with MOG immunohistochemistry after 12 weeks of cuprizone (Figure 11C). This observation is consistent with those of Groebe et al.

(2009) who did not detect cerebellar cortical demyelination using PLP immunohistochemistry or electron microscopy.

The interpretation of these immunohistochemical findings is that hippocampal demyelination is co-incident with CC demyelination, cerebral cortical demyelination is slightly delayed and cerebellar cortical demyelination is not observed in the cuprizone treatment conditions used. Relative to the observed behavioral effects, hippocampal demyelination would be likely to impact functions associated with learning and memory, in contrast to the sensorimotor coordination and social assessments used in the current study targeting CC analysis, or contribute to the epileptic seizures as has also been reported with cuprizone treatment (Hoffman et al., 2008).

Furthermore, the direct effect of cuprizone acute demyelination on CC function has been demonstrated with electrophysiological approaches. Recordings from *ex vivo* slice preparations showed impaired compound action potentials corresponding with acute CC demyelination and that after 6 weeks of cuprizone ingestion subsequent recovery is incomplete after 6 weeks on normal chow (Tiwari-Woodruff et al., 2009). Similarly, cuprizone treatment increased the response latency between left and right cortical neurons and partial recovery was observed after removal of cuprizone from the diet (Bando et al., 2008).

After cuprizone ingestion, the cerebral cortex can also show signs of demyelination with a temporal pattern that is delayed relative to the CC (Skripuletz et al., 2008; Gudi et al., 2009). The complex wheel activity and social interaction changes observed were during acute demyelination at a time when cortical demyelination was not yet evident (Figure 3). Therefore, CC

demyelination may be sufficient for the observed differences in complex wheel activity and social interaction after 6 weeks of cuprizone. The interpretation that impaired CC function is sufficient to cause decreased velocity of running on the complex wheel assay is supported by studies showing similar results with surgical transection of the CC (Schalomon and Wahlsten, 2002).

Extent of cuprizone-induced demyelination pathology in mice

Differences in mouse weight may indicate an underlying variability in the extent of white matter pathology among studies even when a 0.2% cuprizone (w/w) diet is reported. For example, a 30% reduction of weight between treated versus non-treated mice was reported in the study that indicated development of epileptic seizures among the cuprizone treated mice (Hoffman et al., 2008). In the current study, the mice did not lose weight during cuprizone treatment but simply did not gain weight at the same rate as non-treated mice (see methods). Cuprizone has a dose-dependent toxicity effect on mouse weight (Hiremath et al., 1998). Therefore, variations in weight loss among studies may reflect variations in the cuprizone toxicity experienced. These differences may carry over to differences in the extent of white matter pathology and in the general health and behavior with cuprizone treatment as well. For example, during acute cuprizone treatment Liebetantz and Merkler (2006) reported differences in running parameters on the training wheels that were speculated as due to impairment of general health while differences on the training wheels were not observed in the current study. Importantly, the Liebetantz and Merkler study used female C57Bl/6 mice with an average starting weight of 16.5 ± 1.2 g so that the effect of the 0.2% cuprizone dose may have been more severe than in the current study using male C57Bl/6 mice with an average starting weight of 22.42 ± 1.50 g (see methods for other time points).

Use of complementary targeted behavioral CC assays to phenotype mice according to demyelination status

Overall, the resident-intruder social interaction paradigm and the complex wheel running assay can behaviorally phenotype mice according to CC myelination status in the context of the cuprizone model. These non-invasive functional assays can identify affected mice during longitudinal studies. These assays will be especially useful for characterizing acute and chronic disease severity to identify manipulations to promote remyelination. These findings should also facilitate studies to exploit mouse genetics to examine mechanisms of pathogenesis and repair in demyelinating diseases and take advantage of mouse models to determine involvement of the CC in other CNS injuries and disorders.

Implications of this thesis work for MS research

In MS, the potential for remyelination is apparent with the persistence of immature OL cells MS lesions (Maeda et al., 2001; Chang et al., 2002; Wilson et al., 2006; Pasquini et al., 2007). Furthermore, chronic MS lesions retain the capacity for remyelination. However, increased expression of signals that inhibit differentiation (Wolswijk, 1998; Emery et al., 2006) or variable expression of molecules that support newly generated oligodendrocytes to survive and myelinate viable axons (John et al., 2002; Back et al., 2005) might be a factor in MS lesions. This work further shows apoptosis and astrogliosis as cellular mechanisms that can influence the capacity for remyelination especially after prolonged or chronic demyelination. Additionally, combination of the resident-intruder social interaction paradigm with the bilateral sensorimotor complex running wheel assay reliably predicts myelination status in cuprizone treated animals, suggesting use of this non-invasive behavioral assay a method for not only

diagnosing demyelination status in rodents, but also as means of testing novel therapeutics designed to promote functional remyelination. Future studies should focus on the applicability of such assays to other disorders affecting the CC.

Concluding statement

Though promotion of remyelination, possibly through therapeutic manipulation of endogenous mechanisms, is the eventual goal of the studies presented in this work, attaining this goal requires a better understanding of remyelination potential, especially within the context of chronic demyelinating insults. In all the studies presented in this work, the cuprizone model was used as the method to induce demyelination. Research efforts involving human MS tissue or employing other animal models of demyelination indicate that the findings in these studies are pertinent to delineating the mechanisms contributing to remyelination capacity. Furthermore, this research has implications for the design of novel therapeutics in the treatment of MS and other demyelinating disorders.

Bibliography:

Albrecht PJ, Murtie JC, Ness JK, Redwine JM, Enterline JR, Armstrong RC, Levison SW (2003) Astrocytes produce CNTF during the remyelination phase of viral-induced spinal cord demyelination to stimulate FGF-2 production. Neurobiol Dis 13:89-101.

Antel J, Antel S, Caramanos Z, Arnold DL, Kuhlmann T (2012) Primary progressive multiple sclerosis: part of the MS disease spectrum or separate disease entity? Acta Neuropathol.

Armstrong RC, Le TQ, Frost EE, Borke RC, Vana AC (2002) Absence of fibroblast growth factor 2 promotes oligodendroglial repopulation of demyelinated white matter. J Neurosci 22:8574-8585.

Armstrong RC, Le TQ, Flint NC, Vana AC, Zhou YX (2006) Endogenous cell repair of chronic demyelination. J Neuropathol Exp Neurol 65:245-256.

Back SA, Tuohy TM, Chen H, Wallingford N, Craig A, Struve J, Luo NL, Banine F, Liu Y, Chang A, Trapp BD, Bebo BF, Jr., Rao MS, Sherman LS (2005) Hyaluronan accumulates in demyelinated lesions and inhibits oligodendrocyte progenitor maturation. Nat Med 11:966-972.

Barres BA, Hart IK, Coles HS, Burne JF, Voyvodic JT, Richardson WD, Raff MC (1992a) Cell death and control of cell survival in the oligodendrocyte lineage. Cell 70:31-46.

Barres BA, Hart IK, Coles HS, Burne JF, Voyvodic JT, Richardson WD, Raff MC (1992b) Cell death in the oligodendrocyte lineage. J Neurobiol 23:1221-1230.

Breij EC, Brink BP, Veerhuis R, van den Berg C, Vloet R, Yan R, Dijkstra CD, van der Valk P, Bo L (2008) Homogeneity of active demyelinating lesions in established multiple sclerosis. Ann Neurol 63:16-25.

Brenner M, Kisseberth WC, Su Y, Besnard F, Messing A (1994) GFAP promoter directs astrocyte-specific expression in transgenic mice. J Neurosci 14:1030-1037.

Buss A, Pech K, Kakulas BA, Martin D, Schoenen J, Noth J, Brook GA (2007) Growth-modulating molecules are associated with invading Schwann cells and not astrocytes in human traumatic spinal cord injury. Brain 130:940-953.

Chang A, Tourtellotte WW, Rudick R, Trapp BD (2002) Premyelinating oligodendrocytes in chronic lesions of multiple sclerosis. N Engl J Med 346:165-173.

Coffey JC, McDermott KW (1997) The regional distribution of myelin oligodendrocyte glycoprotein (MOG) in the developing rat CNS: an in vivo immunohistochemical study. J Neurocytol 26:149-161.

Crawford DK, Mangiardi M, Xia X, Lopez-Valdes HE, Tiwari-Woodruff SK (2009) Functional recovery of callosal axons following demyelination: a critical window. Neuroscience 164:1407-1421.

Denic A, Johnson AJ, Bieber AJ, Warrington AE, Rodriguez M, Pirko I (2011) The relevance of animal models in multiple sclerosis research. Pathophysiology 18:21-29.

Eddleston M, Mucke L (1993) Molecular profile of reactive astrocytes--implications for their role in neurologic disease. Neuroscience 54:15-36.

Emery B, Cate HS, Marriott M, Merson T, Binder MD, Snell C, Soo PY, Murray S, Croker B, Zhang JG, Alexander WS, Cooper H, Butzkueven H, Kilpatrick TJ (2006) Suppressor of cytokine signaling 3 limits protection of leukemia inhibitory factor receptor signaling against central demyelination. Proc Natl Acad Sci U S A 103:7859-7864.

Fitch MT, Silver J (2008) CNS injury, glial scars, and inflammation: Inhibitory extracellular matrices and regeneration failure. Exp Neurol 209:294-301.

Frost EE, Nielsen JA, Le TQ, Armstrong RC (2003) PDGF and FGF2 regulate oligodendrocyte progenitor responses to demyelination. J Neurobiol 54:457-472.

Fruttiger M, Calver AR, Richardson WD (2000) Platelet-derived growth factor is constitutively secreted from neuronal cell bodies but not from axons. Curr Biol 10:1283-1286.

Fruttiger M, Karlsson L, Hall AC, Abramsson A, Calver AR, Bostrom H, Willetts K, Bertold CH, Heath JK, Betsholtz C, Richardson WD (1999) Defective oligodendrocyte development and severe hypomyelination in PDGF-A knockout mice. Development 126:457-467.

Gallo V, Armstrong RC (2008) Myelin repair strategies: a cellular view. Curr Opin Neurol 21:278-283.

Gard AL, Burrell MR, Pfeiffer SE, Rudge JS, Williams WC, 2nd (1995) Astroglial control of oligodendrocyte survival mediated by PDGF and leukemia inhibitory factor-like protein. Development 121:2187-2197.

Garwood J, Garcion E, Dobbertin A, Heck N, Calco V, ffrench-Constant C, Faissner A (2004) The extracellular matrix glycoprotein Tenascin-C is expressed by oligodendrocyte precursor cells and required for the regulation of maturation rate, survival and responsiveness to platelet-derived growth factor. Eur J Neurosci 20:2524-2540.

Gean-Marton AD, Vezina LG, Marton KI, Stimac GK, Peyster RG, Taveras JM, Davis KR (1991) Abnormal corpus callosum: a sensitive and specific indicator of multiple sclerosis. Radiology 180:215-221.

Grinspan JB, Franceschini B (1995) Platelet-derived growth factor is a survival factor for PSA-NCAM+ oligodendrocyte pre-progenitor cells. J Neurosci Res 41:540-551.

Groebe A, Clarner T, Baumgartner W, Dang J, Beyer C, Kipp M (2009) Cuprizone treatment induces distinct demyelination, astrocytosis, and microglia cell invasion or proliferation in the mouse cerebellum. Cerebellum 8:163-174.

Gudi V, Moharregh-Khiabani D, Skripuletz T, Koutsoudaki PN, Kotsiari A, Skuljec J, Trebst C, Stangel M (2009) Regional differences between grey and white matter in cuprizone induced demyelination. Brain Res 1283:127-138.

Gutowski NJ, Newcombe J, Cuzner ML (1999) Tenascin-R and C in multiple sclerosis lesions: relevance to extracellular matrix remodelling. Neuropathol Appl Neurobiol 25:207-214.

Hamby ME, Sofroniew MV (2011) Reactive astrocytes as therapeutic targets for CNS disorders. Neurotherapeutics 7:494-506.

Hanafy KA, Sloane JA (2011) Regulation of remyelination in multiple sclerosis. FEBS Lett 585:3821-3828.

Hartline DK, Colman DR (2007) Rapid conduction and the evolution of giant axons and myelinated fibers. Curr Biol 17:R29-35.

Haylock-Jacobs S, Keough MB, Lau L, Yong VW (2011) Chondroitin sulphate proteoglycans: extracellular matrix proteins that regulate immunity of the central nervous system. Autoimmun Rev 10:766-772.

Heneka MT, Rodriguez JJ, Verkhratsky A (2010) Neuroglia in neurodegeneration. Brain Res Rev 63:189-211.

Hibbits N, Pannu R, Wu TJ, Armstrong RC (2009) Cuprizone demyelination of the corpus callosum in mice correlates with altered social interaction and impaired bilateral sensorimotor coordination. ASN Neuro 1.

Hinks GL, Franklin RJ (1999) Distinctive patterns of PDGF-A, FGF-2, IGF-I, and TGF-beta1 gene expression during remyelination of experimentally-induced spinal cord demyelination. Mol Cell Neurosci 14:153-168.

Hiremath MM, Saito Y, Knapp GW, Ting JP, Suzuki K, Matsushima GK (1998) Microglial/macrophage accumulation during cuprizone-induced demyelination in C57BL/6 mice. J Neuroimmunol 92:38-49.

Holley JE, Gveric D, Newcombe J, Cuzner ML, Gutowski NJ (2003) Astrocyte characterization in the multiple sclerosis glial scar. Neuropathol Appl Neurobiol 29:434-444.

John GR, Shankar SL, Shafit-Zagardo B, Massimi A, Lee SC, Raine CS, Brosnan CF (2002) Multiple sclerosis: re-expression of a developmental pathway that restricts oligodendrocyte maturation. Nat Med 8:1115-1121.

Kang W, Hebert JM (2011) Signaling pathways in reactive astrocytes, a genetic perspective. Mol Neurobiol 43:147-154.

Karussis D, Grigoriadis S, Polyzoidou E, Grigoriadis N, Slavin S, Abramsky O (2006) Neuroprotection in multiple sclerosis. Clin Neurol Neurosurg 108:250-254.

Kipp M, Clarner T, Dang J, Copray S, Beyer C (2009) The cuprizone animal model: new insights into an old story. Acta Neuropathol 118:723-736.

Klapka N, Muller HW (2006) Collagen matrix in spinal cord injury. J Neurotrauma 23:422-435.

Kotter MR, Stadelmann C, Hartung HP (2011) Enhancing remyelination in disease--can we wrap it up? Brain 134:1882-1900.

Kotter MR, Stadelmann C, Hartung HP (2012) Enhancing remyelination in disease--can we wrap it up? Brain 134:1882-1900.

Koutsoudaki PN, Skripuletz T, Gudi V, Moharregh-Khiabani D, Hildebrandt H, Trebst C, Stangel M (2009) Demyelination of the hippocampus is prominent in the cuprizone model. Neurosci Lett 451:83-88.

Lassmann H (2011) Review: the architecture of inflammatory demyelinating lesions: implications for studies on pathogenesis. Neuropathol Appl Neurobiol 37:698-710.

Ligon KL, Kesari S, Kitada M, Sun T, Arnett HA, Alberta JA, Anderson DJ, Stiles CD, Rowitch DH (2006) Development of NG2 neural progenitor cells requires Olig gene function. Proc Natl Acad Sci U S A 103:7853-7858.

Lindner M, Heine S, Haastert K, Garde N, Fokuhl J, Linsmeier F, Grothe C, Baumgartner W, Stangel M (2008) Sequential myelin protein expression during remyelination reveals fast and efficient repair after central nervous system demyelination. Neuropathol Appl Neurobiol 34:105-114.

Lucchinetti C, Bruck W (2004) The pathology of primary progressive multiple sclerosis. Mult Scler 10 Suppl 1:S23-30.

Lucchinetti C, Bruck W, Parisi J, Scheithauer B, Rodriguez M, Lassmann H (1999) A quantitative analysis of oligodendrocytes in multiple sclerosis lesions. A study of 113 cases. Brain 122 (Pt 12):2279-2295.

Lucchinetti C, Bruck W, Parisi J, Scheithauer B, Rodriguez M, Lassmann H (2000) Heterogeneity of multiple sclerosis lesions: implications for the pathogenesis of demyelination. Ann Neurol 47:707-717.

Lucchinetti CF, Popescu BF, Bunyan RF, Moll NM, Roemer SF, Lassmann H, Bruck W, Parisi JE, Scheithauer BW, Giannini C, Weigand SD, Mandrekar J, Ransohoff RM (2012) Inflammatory cortical demyelination in early multiple sclerosis. N Engl J Med 365:2188-2197.

Maeda Y, Solanky M, Menonna J, Chapin J, Li W, Dowling P (2001) Platelet-derived growth factor-alpha receptor-positive oligodendroglia are frequent in multiple sclerosis lesions. Ann Neurol 49:776-785.

Mason JL, Langaman C, Morell P, Suzuki K, Matsushima GK (2001) Episodic demyelination and subsequent remyelination within the murine central nervous system: changes in axonal calibre. Neuropathol Appl Neurobiol 27:50-58.

Mason JL, Jones JJ, Taniike M, Morell P, Suzuki K, Matsushima GK (2000) Mature oligodendrocyte apoptosis precedes IGF-1 production and oligodendrocyte progenitor accumulation and differentiation during demyelination/remyelination. J Neurosci Res 61:251-262.

Mason JL, Toews A, Hostettler JD, Morell P, Suzuki K, Goldman JE, Matsushima GK (2004) Oligodendrocytes and progenitors become progressively depleted within chronically demyelinated lesions. Am J Pathol 164:1673-1682.

Matsushima GK, Morell P (2001) The neurotoxicant, cuprizone, as a model to study demyelination and remyelination in the central nervous system. Brain Pathol 11:107-116.

Messersmith DJ, Murtie JC, Le TQ, Frost EE, Armstrong RC (2000) Fibroblast growth factor 2 (FGF2) and FGF receptor expression in an experimental demyelinating disease with extensive remyelination. J Neurosci Res 62:241-256.

Millet V, Moiola CP, Pasquini JM, Soto EF, Pasquini LA (2009) Partial inhibition of proteasome activity enhances remyelination after cuprizone-induced demyelination. Exp Neurol 217:282-296.

Milo R, Kahana E (2009) Multiple sclerosis: geoepidemiology, genetics and the environment. Autoimmun Rev 9:A387-394.

Miron VE, Kuhlmann T, Antel JP (2011) Cells of the oligodendroglial lineage, myelination, and remyelination. Biochim Biophys Acta 1812:184-193.

Moore CS, Abdullah SL, Brown A, Arulpragasam A, Crocker SJ (2011) How factors secreted from astrocytes impact myelin repair. J Neurosci Res 89:13-21.

Muliyil S, Krishnakumar P, Narasimha M (2011) Spatial, temporal and molecular hierarchies in the link between death, delamination and dorsal closure. Development 138:3043-3054.

Murtie JC, Zhou YX, Le TQ, Armstrong RC (2005a) In vivo analysis of oligodendrocyte lineage development in postnatal FGF2 null mice. Glia 49:542-554.

Murtie JC, Zhou YX, Le TQ, Vana AC, Armstrong RC (2005b) PDGF and FGF2 pathways regulate distinct oligodendrocyte lineage responses in experimental demyelination with spontaneous remyelination. Neurobiol Dis 19:171-182.

Nakahara J, Aiso S, Suzuki N (2010) Autoimmune versus oligodendrogliopathy: the pathogenesis of multiple sclerosis. Arch Immunol Ther Exp (Warsz) 58:325-333.

Norkute A, Hieble A, Braun A, Johann S, Clarner T, Baumgartner W, Beyer C, Kipp M (2009) Cuprizone treatment induces demyelination and astrocytosis in the mouse hippocampus. J Neurosci Res 87:1343-1355.

Pasquini LA, Calatayud CA, Bertone Una AL, Millet V, Pasquini JM, Soto EF (2007) The neurotoxic effect of cuprizone on oligodendrocytes depends on the presence of pro-inflammatory cytokines secreted by microglia. Neurochem Res 32:279-292.

Payne N, Siatskas C, Barnard A, Bernard CC (2011) The prospect of stem cells as multi-faceted purveyors of immune modulation, repair and regeneration in multiple sclerosis. Curr Stem Cell Res Ther 6:50-62.

Pekny M, Nilsson M (2005) Astrocyte activation and reactive gliosis. Glia 50:427-434.

Perier O, Gregoire A (1965) Electron microscopic features of multiple sclerosis lesions. Brain 88:937-952.

Pollock RA, Richardson WD (1992) The alternative-splice isoforms of the PDGF A-chain differ in their ability to associate with the extracellular matrix and to bind heparin in vitro. Growth Factors 7:267-277.

Prineas JW, Connell F (1979) Remyelination in multiple sclerosis. Ann Neurol 5:22-31.

Prineas JW, Barnard RO, Kwon EE, Sharer LR, Cho ES (1993) Multiple sclerosis: remyelination of nascent lesions. Ann Neurol 33:137-151.

Redwine JM, Armstrong RC (1998) In vivo proliferation of oligodendrocyte progenitors expressing PDGFalphaR during early remyelination. J Neurobiol 37:413-428.

Reich M, Liefeld T, Gould J, Lerner J, Tamayo P, Mesirov JP (2006) GenePattern 2.0. Nat Genet 38:500-501.

Reynolds C, Ratanatharathorn V, Adams P, Braun T, Silver S, Ayash L, Carson E, Eisbruch A, Dawson LA, McDonagh K, Ferrara J, Uberti J (2001) Allogeneic stem cell transplantation reduces disease progression compared to autologous transplantation in patients with multiple myeloma. Bone Marrow Transplant 27:801-807.

Schirmer L, Antel JP, Bruck W, Stadelmann C (2011) Axonal loss and neurofilament phosphorylation changes accompany lesion development and clinical progression in multiple sclerosis. Brain Pathol 21:428-440.

Schonrock LM, Kuhlmann T, Adler S, Bitsch A, Bruck W (1998) Identification of glial cell proliferation in early multiple sclerosis lesions. Neuropathol Appl Neurobiol 24:320-330.

Schwab ME, Bartholdi D (1996) Degeneration and regeneration of axons in the lesioned spinal cord. Physiol Rev 76:319-370.

Silver J, Miller JH (2004) Regeneration beyond the glial scar. Nat Rev Neurosci 5:146-156.

Singh P, Carraher C, Schwarzbauer JE (2010) Assembly of fibronectin extracellular matrix. Annu Rev Cell Dev Biol 26:397-419.

Sobel RA, Mitchell ME (1989) Fibronectin in multiple sclerosis lesions. Am J Pathol 135:161-168.

Sofroniew MV (2009) Molecular dissection of reactive astrogliosis and glial scar formation. Trends Neurosci 32:638-647.

Sofroniew MV, Vinters HV (2010) Astrocytes: biology and pathology. Acta Neuropathol 119:7-35.

Stangel M (2008) Neuroprotection and neuroregeneration in multiple sclerosis. J Neurol 255 Suppl 6:77-81.

Steelman AJ, Thompson JP, Li J (2011) Demyelination and remyelination in anatomically distinct regions of the corpus callosum following cuprizone intoxication. Neurosci Res 72:32-42.

Steelman AJ, Thompson JP, Li J (2012) Demyelination and remyelination in anatomically distinct regions of the corpus callosum following cuprizone intoxication. Neurosci Res 72:32-42.

Tate CC, Garcia AJ, LaPlaca MC (2007) Plasma fibronectin is neuroprotective following traumatic brain injury. Exp Neurol 207:13-22.

Tucker BA, Mearow KM (2008) Peripheral sensory axon growth: from receptor binding to cellular signaling. Can J Neurol Sci 35:551-566.

van der Goes A, Dijkstra CD (2001) Models for demyelination. Prog Brain Res 132:149-163.

van der Valk P, De Groot CJ (2000) Staging of multiple sclerosis (MS) lesions: pathology of the time frame of MS. Neuropathol Appl Neurobiol 26:2-10.

van Heyningen P, Calver AR, Richardson WD (2001) Control of progenitor cell number by mitogen supply and demand. Curr Biol 11:232-241.

Vana AC, Flint NC, Harwood NE, Le TQ, Fruttiger M, Armstrong RC (2007) Platelet-derived growth factor promotes repair of chronically demyelinated white matter. J Neuropathol Exp Neurol 66:975-988.

Williams A, Piaton G, Lubetzki C (2007) Astrocytes--friends or foes in multiple sclerosis? Glia 55:1300-1312.

Wilson HC, Scolding NJ, Raine CS (2006) Co-expression of PDGF alpha receptor and NG2 by oligodendrocyte precursors in human CNS and multiple sclerosis lesions. J Neuroimmunol 176:162-173.

Wolswijk G (1998) Chronic stage multiple sclerosis lesions contain a relatively quiescent population of oligodendrocyte precursor cells. J Neurosci 18:601-609.

Wolswijk G (2000) Oligodendrocyte survival, loss and birth in lesions of chronic-stage multiple sclerosis. Brain 123 (Pt 1):105-115.

Wolswijk G (2002) Oligodendrocyte precursor cells in the demyelinated multiple sclerosis spinal cord. Brain 125:338-349.

Woodruff RH, Fruttiger M, Richardson WD, Franklin RJ (2004) Platelet-derived growth factor regulates oligodendrocyte progenitor numbers in adult CNS and their response following CNS demyelination. Mol Cell Neurosci 25:252-262.

Xie M, Tobin JE, Budde MD, Chen CI, Trinkaus K, Cross AH, McDaniel DP, Song SK, Armstrong RC (2010) Rostrocaudal analysis of corpus callosum demyelination and axon damage across disease stages refines diffusion tensor imaging correlations with pathological features. J Neuropathol Exp Neurol 69:704-716.

Yosef N, Regev A (2011) Impulse control: temporal dynamics in gene transcription. Cell 144:886-896.

Yoshioka N, Hisanaga S, Kawano H (2010) Suppression of fibrotic scar formation promotes axonal regeneration without disturbing blood-brain barrier repair and withdrawal of leukocytes after traumatic brain injury. J Comp Neurol 518:3867-3881.

Zhang D, Hu X, Qian L, O'Callaghan JP, Hong JS (2010) Astrogliosis in CNS pathologies: is there a role for microglia? Mol Neurobiol 41:232-241.

Zhao C, Fancy SP, Magy L, Urwin JE, Franklin RJ (2005) Stem cells, progenitors and myelin repair. J Anat 207:251-258.

Zhou YX, Flint NC, Murtie JC, Le TQ, Armstrong RC (2006) Retroviral lineage analysis of fibroblast growth factor receptor signaling in FGF2 inhibition of oligodendrocyte progenitor differentiation. Glia 54:578-590.